The Dissertation Committee for Seohee Kim Certifies that this is the approved version of the following dissertation:

Polarization and Charge Transport in Polymer and 2-D Material Based Field-Effect Transistors

Committee:

Ananth Dodabalapur, Supervisor

Jack Lee

Seth R. Bank

Deji Akinwande

Hu Tao

Polarization and Charge Transport in Polymer and 2-D Material Based Field-Effect Transistors

by

Seohee Kim, B.S.; M.S.E.E.

Dissertation

Presented to the Faculty of the Graduate School of

The University of Texas at Austin

in Partial Fulfillment

of the Requirements

for the Degree of

Doctor of Philosophy

The University of Texas at Austin

December 2016

Dedication

To my beloved parents, Byoungouk Kim and Yoonok Lee

Acknowledgements

First of all, I would like to deeply appreciate my supervisor, Prof. Ananth Dodabalapur for his excellent support and guidance for my Ph.D. course. I would also like to thank my dissertation committee members, Prof. Jack Lee, Prof. Seth R. Bank, Prof. Deji Akinwande and Prof. Hu Tao for their constructive advice on my dissertation. I would like to thank all of the present and former members of Dodabalapur research group: Dr. Taeho Jung, Dr. Davianne Duarte, Dr. Leander Schulz, Dr. Tae-Jun Ha, Dr. Eric Danielson, Dr. Bongjun Kim, Dr. Seonpil Jang, Dr. Barrett Worley, Dr. Oleksiy Slobodyan, Rohit Yadav, Xin Xu, Kelly Liang, Michael Rodder and Xiao Wang for valuable discussions, brainstorming, and helping in the lab. In particular, I appreciate Dr. Jang for useful discussions and support on my graduate school life, and Dr. Slobodyan for his help on my writing and presentation. I would also like to acknowledge Saungeun Park for helpful discussions and his great support on my device fabrication. Thanks goes out to the Microelectronics Research Center staff, especially Jo Ann Smith, and all my Korean colleagues, for all of their support. Finally, I acknowledge the support from NASCENT and NSF ECCS Division.

Polarization and Charge Transport in Polymer and 2-D Material Based Field-Effect Transistors

Seohee Kim, Ph.D.

The University of Texas at Austin, 2016

Supervisor: Ananth Dodabalapur

This work investigates new semiconductors that are currently being considered for use in flexible electronics. It is critical to understand charge transport physics in field-effect transistors (FETs) to get better device performance and integrate them into commercial products. The charge transport studies include understanding of effect of wide-range of applying voltage (sub-threshold and above threshold operation), dominant charge transport mechanisms under specific conditions (band, band-like and hopping transport), and of polarization effect (polaronic and non-polaronic transport).

Charge transport in high-mobility diketopyrrolopyrrole (DPP) co-polymers FETs is investigated. Sub-threshold regime conduction, including diffusion- and drift-limited regimes, are accurately modeled with above threshold regime. Based on modeling results, the realistic density of states (DOS) curve of polymer FETs in a wide range of gate voltages is calculated. From modeled sub- and above- threshold regime mobility data, dominant charge transport mechanisms under specific conditions are investigated. Shallow states charge transport is well-described by multiple trap and release (MTR) transport, while hopping transport models such as variable range hopping (VRH) or Gaussian disorder based model (GDM) can describe deep states charge transport. The transition between the conduction regimes is a function of temperature and carrier density. In addition, a

polarization effect from polar molecules in both atmosphere and dielectric on the electronic properties of polymer FETs is demonstrated. High-*k* and low-*k* surface dielectric devices are measured in polar and non-polar atmospheres. Dipoles in both conditions affect conduction in polymer FETs, but have different aspects, such as uniformly shifted DOS or only shallow states shifted DOS.

The improved electrical characteristics of graphene monolayer sheet FETs with fluoropolymer capping is explained via measurements under polar vapor flow, which is reversible and non-destructive. It is found that the higher dipole moment of polar molecules corresponds to better improvement of electrical properties of graphene FETs, including the Dirac voltage shift, mobility and residual carrier concentration. In addition, a similar experiment is applied to graphene nano-ribbon (GNR) FETs. GNR FETs, which have high on/off ratio but some degraded electrical characteristics due to a considerable number of edge defects, also show a highly improved performance under polar vapor.

Table of Contents

List of Tables

List of Figures

Chapter 1. Introduction

Chapter 1 surveys the major organic/polymer and graphene materials which are reported on in this work, and introduces the major concepts and topics discussed in subsequent chapters.

Organic/polymer transistor-based circuits have been highlighted for research interest over the last three decades due to their unique properties and potential for use in large-area, low-cost applications, particularly those that are compatible with flexible circuits [1-5]. Organic/polymer field-effect transistors (FETs) have been proposed for applications such as display switches, display drivers, radio-frequency identification (RFID) tags, and sensors. Polymer transistors have also been integrated with optical devices such as light-emitting diodes (LEDs), electrophoretic cells, and liquid crystals, as illustrated in Figure 1.1 and 1.2 [6-14]. Among a number of potential candidates, diketopyrrolopyrrole (DPP) co-polymers are particularly promising on account of their high mobility, often exceeding 2 cm^2/Vs [15-22].

Two-dimensional (2-D) atomic sheets are also good candidates for flexible electronics [23]. These 2-D material based semiconductors are atomically thin-layered crystalline solids. The characteristics of 2-D semiconductors are determined by intralayer covalent bonding and interlayer van der Waals bonding [24-26]. A variety of 2-D semiconductors is shown on Figure 1.3a. The 2-D materials are good for a number of applications such as semiconductors, insulators, transparent conductors and transducers [26-28]. Additionally, 2-D semiconductors can enable flexible electronic applications because they are accessible on soft polymeric or plastic substrates, as shown on Figure 1.3 [29-33].

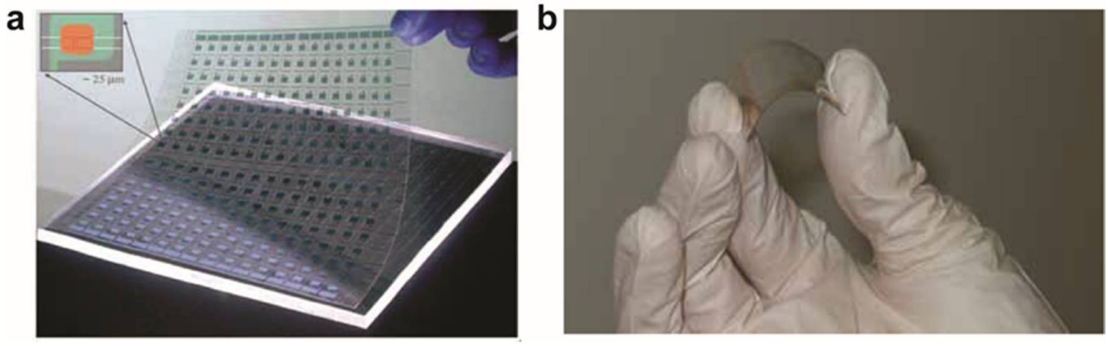

Figure 1.1: (a) The backplane for a 256-element electronic paper system based on an organic semiconductor with channel length < 20 um in each pixels [34]. (b) Photo of an RFID tag component circuit (Courtesy of OrganicID Corporation).

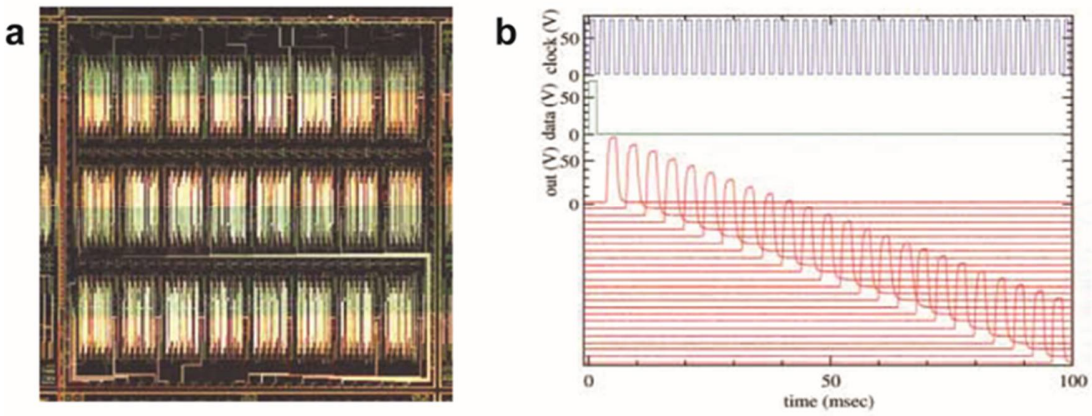

Figure 1.2: (a) Photograph of an 864-transistor organic complementary shift register with 48 stages. The bluish regions contain the n-channel $F_{16}CuPc$ transistors and the yellow regions contain the p-channel oligothiophene transistors. (b) The electrical response of the 48-stage shift register. The output of alternate stages (24 in all) is shown vertically offset for clarity. The clock rate is 1 kHz [3].

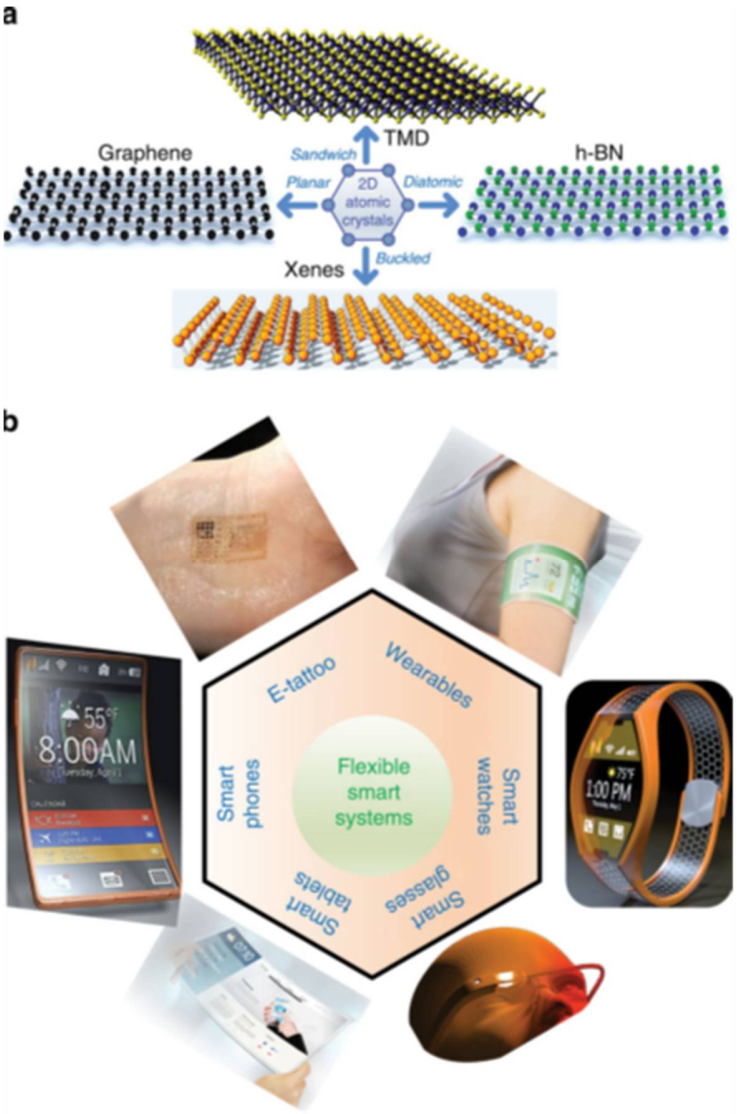

Figure 1.3: (a) Three-dimensional illustrations of contemporary 2-D monolayer materials revealing diverse physical structures based on an underlying hexagonal lattice. (b) 2-D atomic sheets can fulfil many of the electronic, optical and mechanical functions required in a flexible smart system, and especially enable 'RF wireless communication & connectivity,' which has become an indispensable feature in modern smart systems. (Image of the smart tablet and wearable system courtesy of Graphene Square Inc.; Image of smart glasses courtesy of E. Guy; Image of E-tattoo courtesy of N. Lu, University of Texas at Austin) [23].

1.1 POLYMER FIELD-EFFECT TRANSISTOR

1.1.1 Charge Transport in Polymer FET

Several models are used to explain charge transport in polymer FETs. First, the multiple trap and release (MTR) model is most widely used to describe the charge transport in high mobility polymer FETs as well as amorphous silicon thin-film transistors (TFT). In the MTR model, a narrow delocalized band is associated with a high concentration of localized levels that act as traps [15, 35-37]. The charge carriers interact with the localized levels through trapping and thermal release during their transit through the delocalized band level. The following assumptions are usually made: First, the carriers arriving at a trap are instantaneously trapped with a probability close to one. Second, the release of trapped carriers is controlled by a thermally activated process. The resulting mobility μ_{FET} of FET is related to the mobility $\mu_{0,\mathrm{MTR}}$ in the delocalized band by an expression of the form in (eq 1.1).

$$\mu_{\mathrm{FET}} = \mu_{0,\mathrm{MTR}} \exp\left(-\frac{E_A}{kT}\right) \qquad \text{(eq 1.1)}$$

where E_{A} is the activation energy and kT is a thermal voltage. In the case of a single trapping level, E_{A} corresponds to the distance between the trap level and the delocalized band edge. (eq 1.1) shows that Arrhenius type behavior is characteristic of MTR transport. Figure 1.4 illustrates MTR transport in both N- and P-type semiconductors.

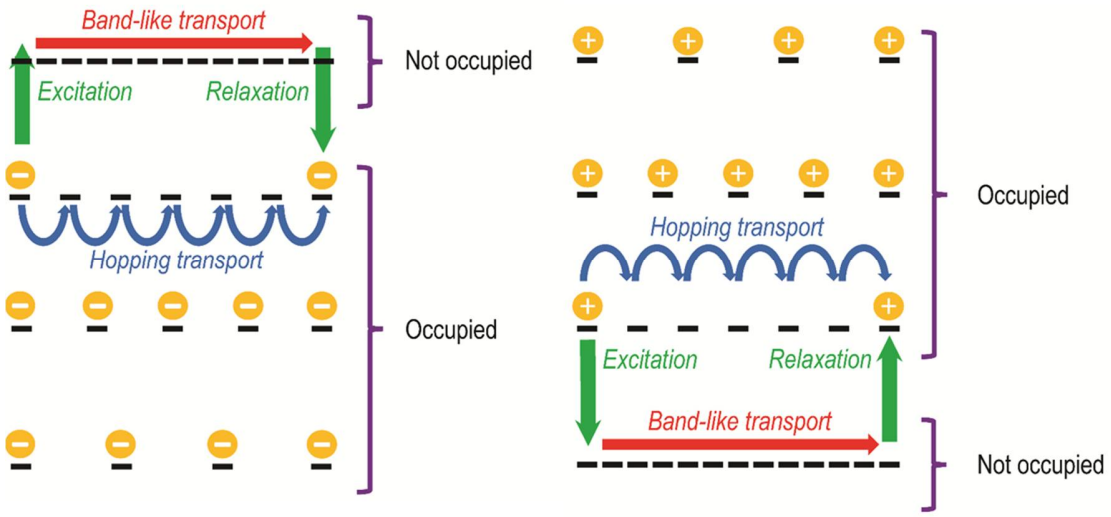

Figure 1.4: Visual description of MTR transport mechanism in N-type (left) and P-type (right) semiconductor FETs.

In addition to MTR, hopping transport models are used to describe charge transport in polymer FET, especially for the case of low mobility materials. There are two established hopping transport models: variable range hopping (VRH) and Gaussian disordered model (GDM). The VRH theory is based on the idea that charges are localized but can hop to another localized state [35, 38-41]. The probability of hopping between two states of spatial separation R and energy separation W is given by (eq 1.2) [40].

$$P(R,W) = \exp\left(-aR - \frac{W}{kT}\right) \qquad \text{(eq 1.2)}$$

with k is Boltzmann's constant, and a is a constant. The total conduction can then be found as the integral over all energy states and distances, which can be worked out into the Mott's famous VRH equation with conductivity proportional to $\exp[-(T_0/T)^{1/4}]$, in three-

dimensions. In terms of field-effect mobility, the VRH mobility is related to temperature by the (eq 1.3) [41].

$$\mu_{\mathrm{FET}} = \frac{\mu_{\mathrm{REF,VRH}}}{T^{1.5}} \exp\left[-\left(\frac{D}{kT} \right)^{0.25} \right] \qquad \text{(eq 1.3)}$$

In case of the Gaussian disorder model (GDM) proposed by Bässler et al., carriers hop through a Gaussian density of transport states of energetic width σ via Miller-Abrahams hopping rates [42-45]. The main difference between VRH and GDM model is that the energetic distribution of traps: which are randomly distributed in VRH, whereas possess a Gaussian distribution in the GDM. The field-effect mobility for GDM is given by the (eq 1.4):

$$\mu_{\mathrm{FET}} = \mu_{\mathrm{REF,GDM}} \exp\left[-C\left(\frac{\sigma}{kT} \right)^{2} \right] \qquad \text{(eq 1.4)}$$

Figure 1.5 describes hopping transport process in both N- and P-type semiconductors. Hopping transport is dominant within the deep states, meaning that the trap states are located far from the delocalized band edge level. For carriers occupying shallow trap states, MTR is likely to be a dominant transport mechanism as the extended states are more easily accessible to them, as shown in Figure 1.4.

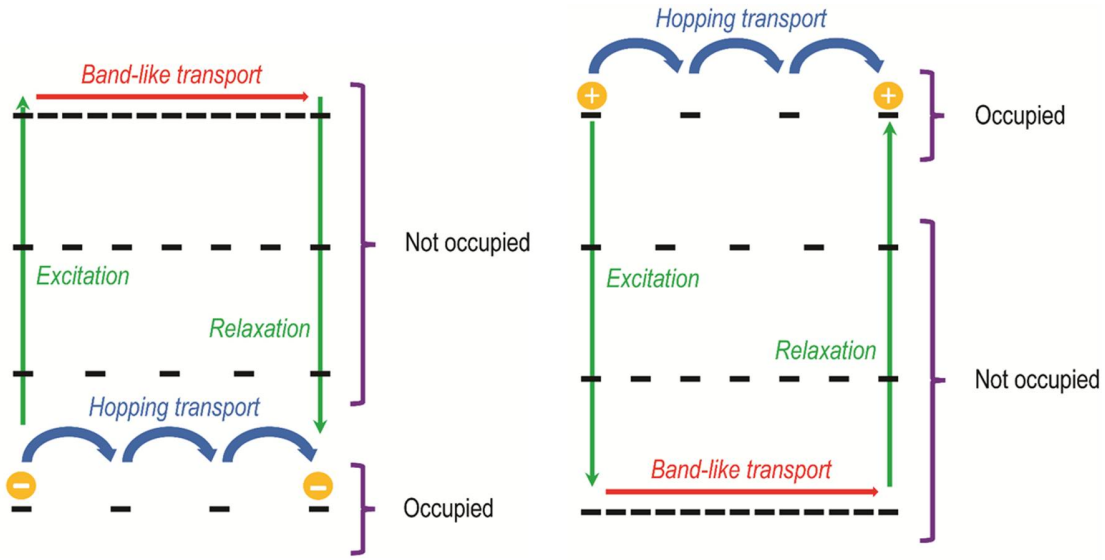

Figure 1.5: Visual description of hopping transport mechanism in N-type (left) and P-type (right) semiconductor FETs.

1.1.2 Sub-threshold Characteristics

Polymer semiconductors are typically disordered and have many deep bulk trap states, located principally at domain/grain boundaries in the active layer, even in semi-crystalline film, as shown in Figure 1.6 [42, 46-48]. The sub-threshold region of operation for polymer FETs consists of two different regimes: the diffusion-limited and drift-limited regimes, both shown in Figure 1.7. The diffusion-limited regime is observed in all field-effect transistors and its extent is enhanced by interface traps at the interface between the dielectric and active semiconductor layers. Applying a gate-source voltage (V_{GS}) causes the interface traps to become occupied by carriers prior to the bulk traps due to band bending. Therefore, as shown in Figure 1.7(a), the diffusion-limited regime appears in the low V_{GS} sub-threshold regime. The diffusion-limited sub-threshold current can be described as follows (eq 1.5) [49, 50]:

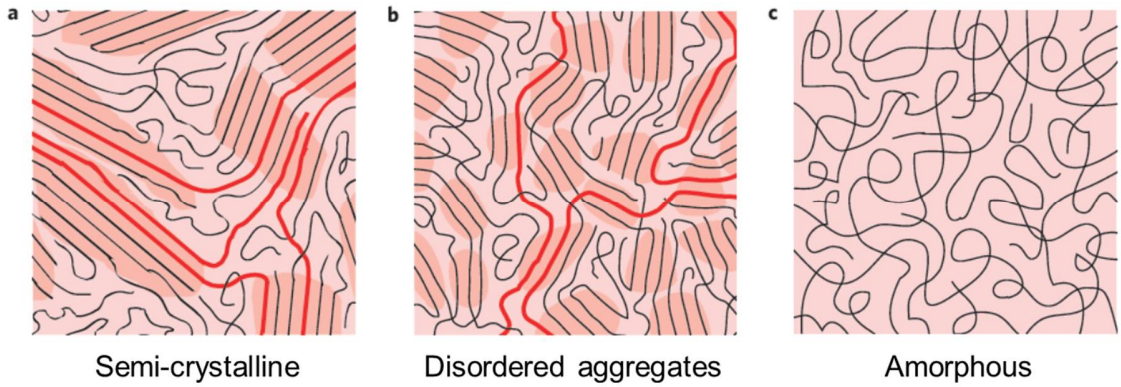

Figure 1.6: Microstructure of conjugated polymer films. Illustrations of the microstructure of a semi-crystalline polymer film, for example P3HT (a), disordered aggregates (b) and a completely amorphous film (c). Note the coexistence of ordered (darker shadowed areas) and spaghetti-like amorphous regions. This microstructure is similar to the concept of fringed micelles. If the molecular weight is high enough and there is a large enough density of ordered material, long polymer chains (highlighted in red) can connect ordered regions without a significant loss of conjugation, greatly improving charge transport [47].

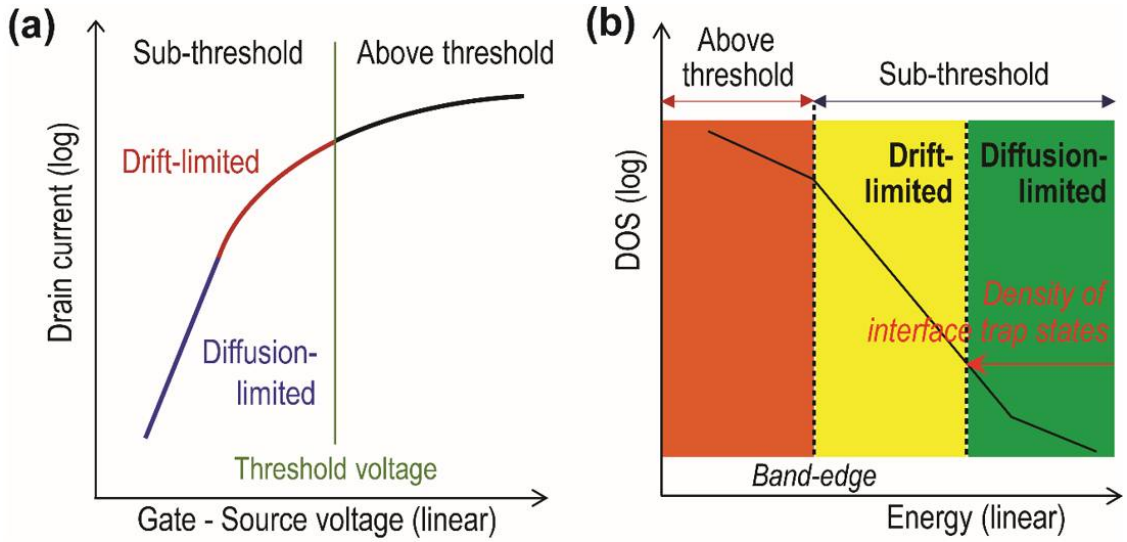

Figure 1.7: Different conduction regimes of polymer transistors as seen from (a) the transfer characteristics and (b) the electronic density of states (DOS) [50].

$$I_{\mathrm{D,Sub,Diff}} \approx I_{\mathrm{Off}} \exp\left[\frac{q}{kT}\left(\frac{\left|V_{\mathrm{GS}}-V_{\mathrm{FB}}\right|}{1+q^2 D_{\mathrm{it}}/C_{\mathrm{i}}}\right)\right] \qquad \text{(eq 1.5)}$$

where q is the elementary charge, kT/q is the thermal voltage, V_{FB} is the flat band voltage, I_{Off} is the off current at $V_{\mathrm{GS}} = V_{\mathrm{FB}}$, C_{i} is the capacitance per unit area, and D_{it} is the interface trap density. V_{ON}, the gate voltage at the onset of conduction, can be used for the value of V_{FB}. In addition to the diffusion-limited regime, polymer FETs also have a pronounced drift-limited sub-threshold regime due to the existence of bulk trap states. The drift-limited current appears in the high V_{GS} sub -threshold region, as shown in Figure 1.7(a). The linear region drift-limited sub-threshold current can be described as follows (eq 1.6) [49, 50]:

$$\begin{aligned} I_{\mathrm{D,Sub,Drift}} &\approx \mu_{\mathrm{FET,Drift}} \frac{W}{L} C_{\mathrm{i}} \left|V_{\mathrm{GS}}-V_{\mathrm{FB}}\right| \left|V_{\mathrm{DS}}\right| \\ &= \beta_{\mathrm{Drift}} \frac{W}{L} C_{\mathrm{i}} \left|V_{\mathrm{GS}}-V_{\mathrm{FB}}\right|^{\alpha_{\mathrm{d}}+1} \left|V_{\mathrm{DS}}\right| \end{aligned} \qquad \text{(eq 1.6)}$$

where W/L is the ratio of channel width to channel length, $\mu_{\mathrm{FET,Drift}}$ is the drift-limited regime field-effect mobility, α_{d} is a power law factor, β_{Drift} is a pre-factor for a drift-limited regime mobility, and V_{DS} is the drain-source voltage. α_{d} can be extracted from the slope of $\log(I_{\mathrm{D,Sub,Diff}})$ vs. $\log|V_{\mathrm{GS}}-V_{\mathrm{FB}}|$ plot (slope = $\alpha_{\mathrm{d}}+1$). When the other parameters are fixed, it is possible to calculate β_{Drift} by fitting data to (eq 1.6). If the transistor operates in a saturation region, then V_{DS} can be expressed as $\gamma_{\mathrm{Sat}}(V_{\mathrm{GS}}-V_{\mathrm{FB}})$, where γ_{Sat} is a saturation factor.

1.1.3 Polarization Effect

Most of polymer semiconductors are polarizable materials with localization and polarization dominating the transport physics [51]. A polaron is a quasiparticle consisting of a charge carrier and the lattice deformation that lowers the mobility and increases the effective mass, as shown in Figure 1.8. The polarization effects in polymer FETs can be originated from polar molecules in atmosphere [52] and in gate dielectric [53] that can affect charge transport in semiconductors. When the semiconductor interacts with a polar molecule, there is enhanced self-trapping of charges, leading to a reduction in drain current, as shown on Figure 1.9(a). Previous work has shown the degree of the semiconductor – polar molecule interaction is related to the number of grain boundaries in the active layer, with the lower mobility devices containing more grain boundaries than the more ordered higher mobility devices [9, 52, 54]. Figure 1.9(b) shows the modification of the carrier trapping energies, which includes molecular polaron effects (self-trapping), disorder induced modification of the DOS, and polar analyte effects.

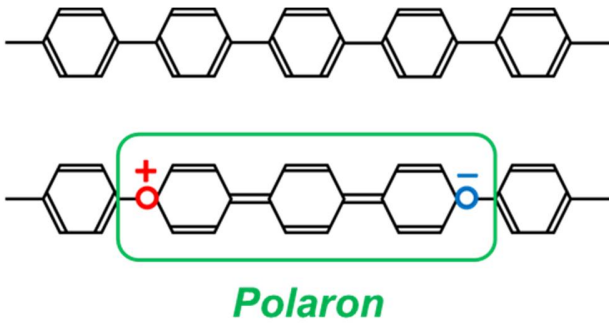

Figure 1.8: Example of polaron quasiparticle formed in polymer chain.

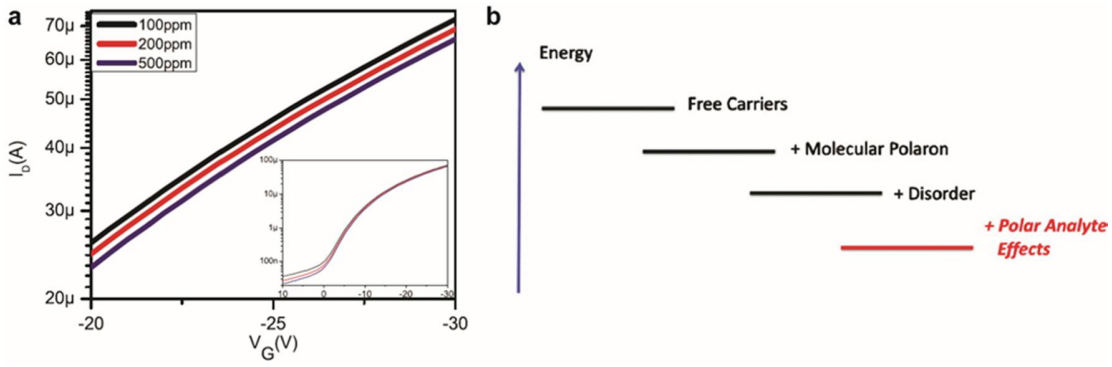

Figure 1.9: (a) Transfer characteristic at $|V_{DS}|$ = 40 V plotted between $|V_{GS}|$ = 20 V and 30 V for pentacene TFT (0.5 cm^2/Vs) showing decreasing current with ethanol concentrations increasing from 100 to 500 ppm. The full transfer characteristics are inset. (b) Modification of the carrier trapping energies including molecular polaron effects (self-trapping), disorder induced modification of the DOS, and polar analyte effects [52].

1.2 GRAPHENE FIELD-EFFECT TRANSISTOR

1.2.1 Charge Transport in Graphene FET

Theoretical calculations predict extremely high carrier mobility for pristine, intrinsic graphene, which is, when ungated, free of doping. Graphene has no band gap, and instead the bands meet at the charge neutral Dirac point [55, 56]. In reality, adventitious doping is very difficult to avoid during normal semiconductor fabrication processes [55, 57, 58]. Generally, experimentally realized graphene is deemed extrinsic, having some amount of free carriers induced by doping from charged impurities and defects, which are present either at the graphene/substrate interfaces or within close proximity to the interfaces [55, 57, 59]. Such impurities can include, among others, adsorbed water or oxygen, residues left over from the wet transfer of graphene to the substrate, ions trapped between the graphene and substrate, and dangling bonds from the SiO_2. Impurities affect the electronic transport of graphene by two principal mechanisms: short-range scattering

and Coulombic, long-range scattering [55, 56, 60]. It is widely agreed that long-range scattering by impurities plays the dominant role in graphene transport for most experimental conditions, given that many as-fabricated samples possess a high concentration of charged impurities [55, 61-64]. Thus, it is imperative for the advancement of graphene microelectronics technology that methods be developed for mitigating the effects of any possible charged impurities and defects. The effect of impurity doping on the characteristics of graphene FET is shown on Figure 1.10.

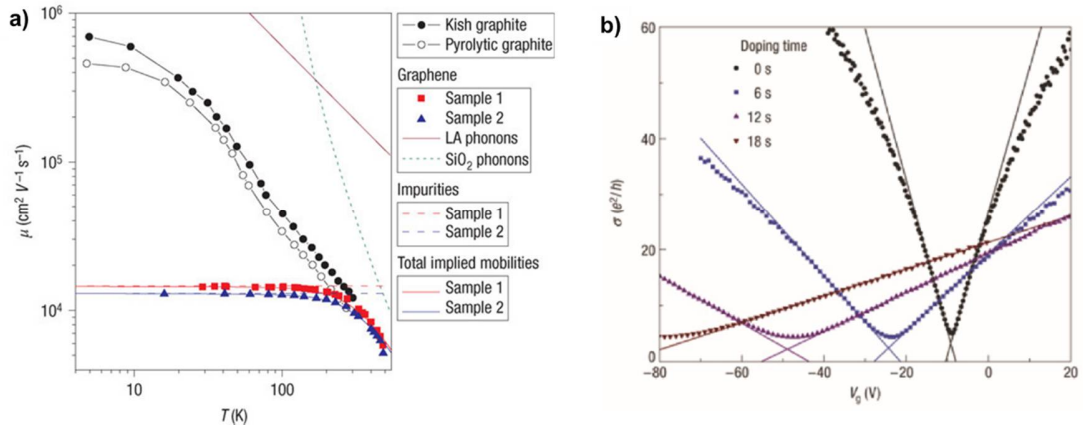

Figure 1.10: (a) Temperature-dependent mobilities of graphene samples 1 and 2 at V_{GS} = 14 V (n = 10^{12} cm^{-2}) are compared with Kish and pyrolytic graphite. The mobility limits in graphene determined in this work for scattering by LA phonons, remote interfacial phonon scattering, and impurity scattering are shown. Red and blue solid lines show the expected net mobility for each sample, according to Matthiessen's rule [58]. (b) Effect of potassium doping of graphene. The conductivity (σ) versus gate voltage (V_{GS}) curves for the pristine sample and three different doping concentrations taken at 20 K in UHV. The crossing of the lines defines the points of the residual conductivity and the gate voltage at minimum conductivity [64].

1.2.2 Effect of Fluoropolymer

A number of previous works have shown that the use of a fluoropolymer thin film atop a graphene monolayer favorably altered the electrical properties of the graphene FETs, enhancing mobility while reducing both carrier concentration and the magnitude of the Dirac voltage, as shown on Figure 1.11 [62, 63]. A possible cause of such electrical property improvements is the neutralization or screening of charged impurities and defects by electrostatic- or van der Waals-type interaction with the dipoles of fluoropolymer C-F bonds. Upon observing that higher annealing temperatures led to both better molecular ordering in thin films and improved electrical properties, it can be also inferred that the self-organization of the fluoropolymer C-F bonds atop the graphene alters the local dielectric environment, as shown on Figure 1.11 [60, 62, 63, 65]. It is expected that modification of the dielectric environment adjacent to graphene will alter the dimensionless coupling constant (also known as the effective fine-structure constant), α, of the graphene system.

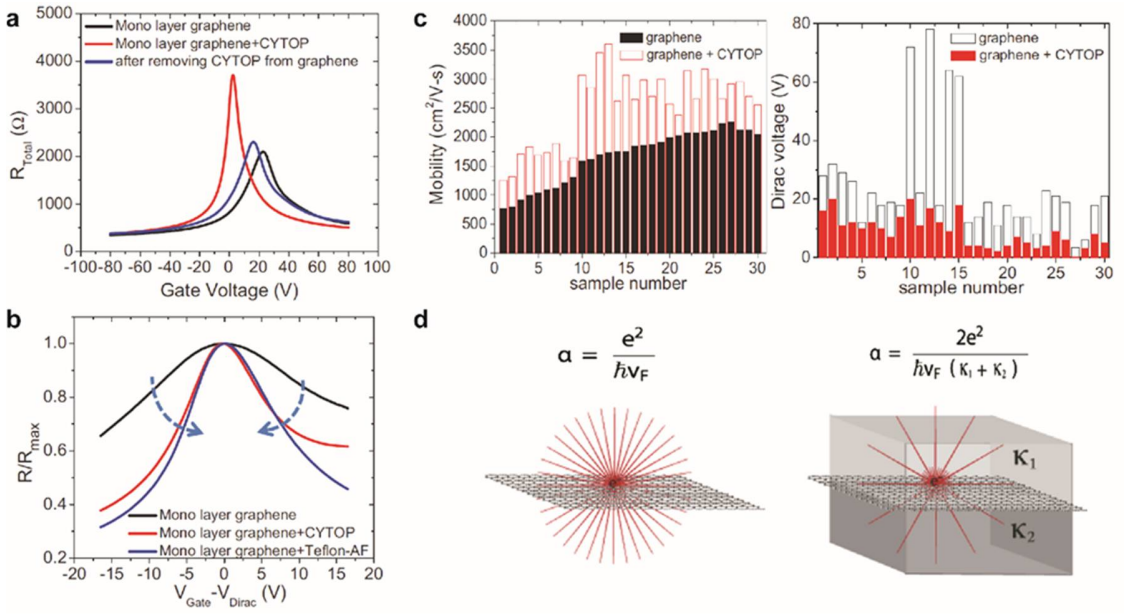

Figure 1.11: (a) Transfer characteristics of monolayer graphene, graphene with CYTOP capping layer and graphene FETs after removing CYTOP. (b) Normalized resistance of mono-layered graphene by capping with fluoropolymer. (c) Device statistics of electrical characteristics of mono-layer graphene FETs before and after capping with CYTOP. (d) Schematic illustrating dielectric screening in graphene. The dielectric environment controls in the interaction strength parametrized by the coupling constant α [60, 63].

1.2.3 Graphene Nano-ribbon Field-Effect Transistor

If graphene is patterned into a narrow ribbon, the carriers may be confined to a quasi-one-dimensional (1-D) system which leads to the opening of an energy gap, as shown on Figure 1.12. Similar to a carbon nano-tube (CNT), this energy gap depends on the width and crystallographic orientation of the graphene nano-ribbon (GNR) [66-68]. In addition, the edge shape of GNR, armchair or zigzag, is also a determinant of bandgap of GNR. The bandgap formation in GNR is helpful for increasing the on-off current modulation of graphene FETs.

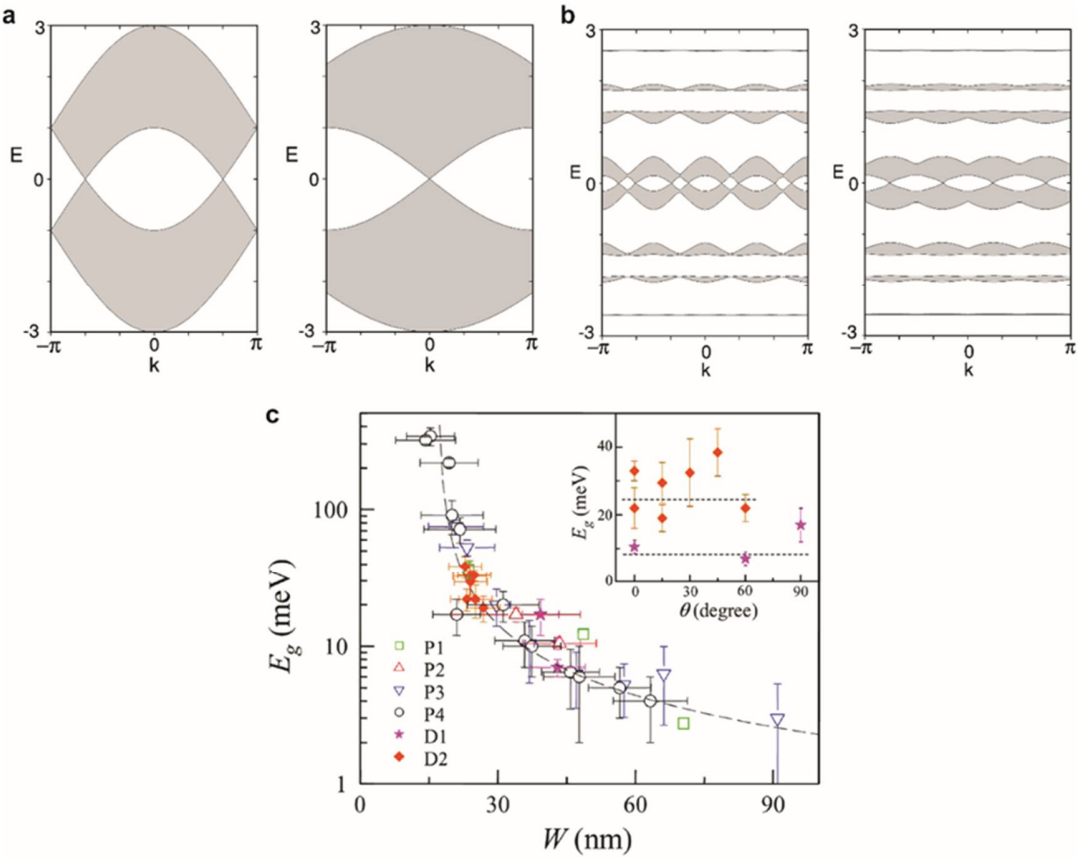

Figure 1.12: (a) The energy band structure of graphite sheet projected to zigzag axis (left) and armchair axis (right) in the absence of the magnetic field. (b) The energy band structure of the graphite sheet projected to zigzag axis (left) and armchair axis (right) for $\phi = 1/4$. (c) E_{gap} vs W for four (P1–P4) of the parallel type and two (D1, D2) with varying orientation. The inset shows E_{gap} vs relative angle θ for the device sets D1 and D2. Dashed lines in the inset show the value of E_{gap} as predicted by the empirical scaling of E_{gap} vs W [66, 67].

However, GNRs are substantially different from CNTs by having two open edges at both sides. These edges not only remove the periodic boundary condition along the circumference of CNTs, but also make GNRs more vulnerable to defects than CNTs [69, 70]. In fact, nearly all observed graphene edges contain local defects or extended disorders, while few defects are found in the bulk of graphene sheets [71]. These edge defects can significantly affect the electronic properties of GNRs. Figure 1.13 shows that the conductance of GNR is critically affected by very few number of atom vacancies. Therefore, the ability to ameliorate the effects of charged impurities and restore the material will have more dramatic effect for GNRs than graphene sheet, and greatly enhance the usefulness of GNRs.

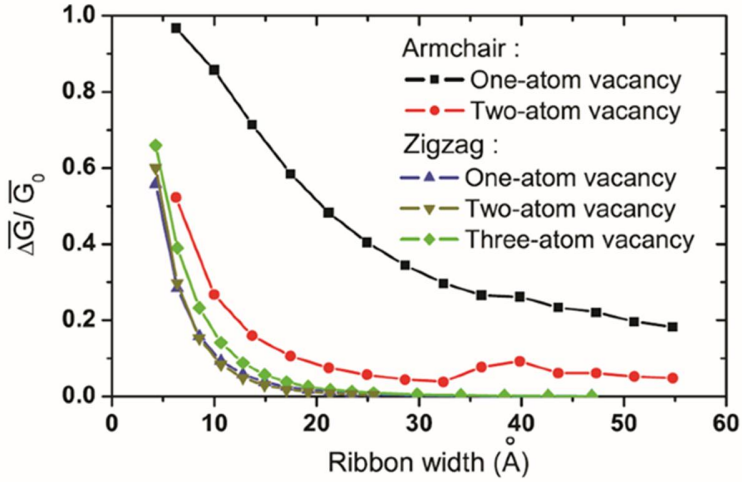

Figure 1.13: The decreasing rate of the average conductance (between ± 0.5 eV) by a single vacancy at the edge. As the width of a zigzag ribbon increases, its conductance becomes immune from a vacancy at its edge [68].

1.3 ORGANIZATION OF DISSERTATION

The purpose of this dissertation is to describe charge transport physics in polymer and graphene FETs in detail and improved electrical properties of graphene nano-ribbon FETs.

This dissertation is divided into seven chapters. Chapter 2 describes a modeling process of electrical characteristics of polymer FETs, mostly focusing on sub-threshold behavior, including an accurate calculation of density of trap states based on the drift-limited regime sub-threshold field-effect mobility values from the modeling result.

Chapter 3 describes a dominant charge transport mechanisms in polymer FETs under certain conditions. To find out the dominant transport mechanism, a modeling technique described in Chapter 2 is applied to get field-effect mobility values. A measured data from polymer FET under wide gate voltage (V_{GS}) range and temperature is used.

Chapter 4 describes the polarization effect on charge transport in polymer FETs. Both polarization effects from atmosphere and gate dielectric are investigated, via analysis on the measured polymer FET electrical data under N_2/Ethanol 2,000 ppm atmosphere and high-*k* ZrO_2/Low-*k* SiO_2 gate dielectric surface.

Chapter 5 describes the effect of polar analyte molecules on the electrical characteristics of graphene FETs, and serves as an illustration of the basic physics of the effect of fluoropolymer coating on graphene FET. Graphene FET is measured under constant vapor flow of a number of polar molecules with different dipole moments. Reversibility of experiment is also discussed.

Chapter 6 describes a method of patterning 10-20 nm scale graphene nano-ribbons from CVD-grown transferred monolayer graphene via e-beam lithography. In addition, electrical characteristics of FETs with GNRs and polar analytes effect on the performance of GNR FETs are discussed.

Finally, Chapter 7 summarizes the conclusions drawn from this research and presents recommendations for future work.

Chapter 2. Sub-threshold Conduction in Polymer FET*

2.1 INTRODUCTION

It has become important to obtain a detailed understanding of charge carrier transport in polymer field-effect transistors [35, 36, 73-76]. The measurement of the density of trap states (DOS) in polymer FETs is one of the key steps in understanding and describing carrier transport phenomena [77-82]. Previous work by D. V. Lang et al. [77] and W. Kalb et al. [79, 80] have used only the above-threshold characteristics to calculate the DOS of an organic single crystal semiconductor. This approach may work fairly well for single crystals in which the density of trap states is small. In polymer field-effect transistors, as well as other thin-film transistors in which there is a lot of disorder, sub-threshold conduction plays an important role even at fairly high gate voltages and must be part of the analysis.

In this chapter, an approach which combines sub-threshold response as well as above threshold response in determining the density of trap states will be discussed. It gives a more accurate DOS of polymer FET over wide gate voltage range including sub-threshold regime by applying drift-limited regime mobility values, as mentioned in Chapter 1.1.2.

* This chapter is based on Reference [72] S. Kim, T.-J. Ha, P. Sonar, and A. Dodabalapur, "Density of trap states in a polymer field-effect transistor," *Applied Physics Letters,* vol. 105, p. 133302, 2014. S.K. and A.D. conceived the idea and designed the experiments. T.-J.H. carried out fabrication of the device. P.S. synthesized the polymer. S.K. carried out characterization of devices and analyzed data.

2.2 EXPERIMENTAL

Data from the thiophene-flanked DPP copolymer with thienylene-vinylene-thienylene (PDPP-TVT) FET is used for analysis [15]. The chemical structure of PDPP-TVT and the device structure of the FET are shown on Figure 2.1(a) and (b), respectively. N-doped silicon was used as gate, with 290 nm thermally grown SiO_2 dielectric layer. The dielectric layer gave a value of capacitance per unit area (C_i) of 12 nF/cm^2. PDPP-TVT film was spin coated on octadecyltrichlorosilane (ODTS) self-assembled monolayer (SAM) treated surface and annealed under an inert atmosphere at 200˚C for 30 min. The Ti/Au (2.5 nm/45 nm) source/drain electrodes were deposited on the polymer layer by thermal evaporation. The electrical characteristics of the FET were measured at both 300 K and 273 K, using a semiconductor parameter analyzer in a cryogenic probe station. The channel width (W) and length (L) of the FET is 1000 μm and 50 μm, respectively.

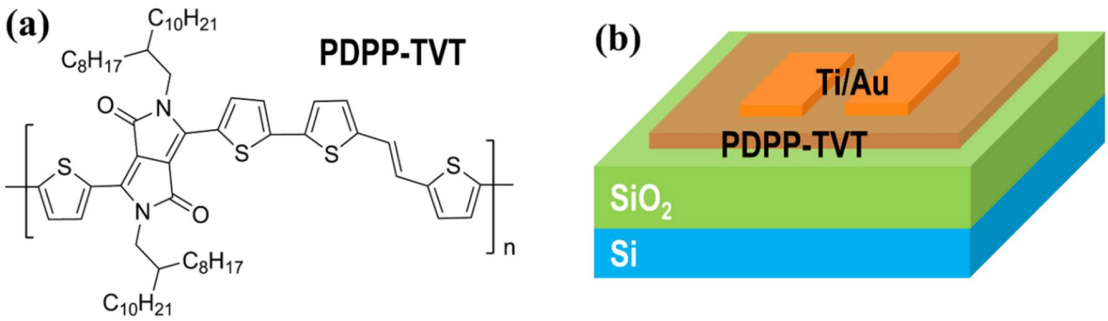

Figure 2.1: (a) The chemical structure of PDPP-TVT, (b) device structure of PDPP-TVT FET.

2.3 RESULT AND DISCUSSION

2.3.1 Drift-limited Regime

The transfer curves of PDPP-TVT FET at a drain-source voltage V_{DS} = – 10 V are shown in Figure 2.2. First, the threshold voltages (V_T) is extracted from a linear drain current (I_D) vs. a gate-source voltage (V_{GS}) plot to define sub-threshold and above-threshold regimes. V_T at 300 K and 273 K are – 35.6 V and – 37.6 V, respectively. In previous work from other groups, there was no specified method for identifying the sub-threshold regime [77]. The Sub-threshold Swing (S.S.) was used to calculate the constant interface trap states density [80, 83]. This method works quite well for single crystal organic TFTs which typically have a relatively small number of deep trap states. However, the presence of a significant drift-limited sub-threshold regime is a characteristic of disordered semiconductor based FETs and must be taken into consideration in determining the density of trap states. PDPP-TVT FET clearly possess a wide range in which there is a non-linear semi-log I_D vs. V_{GS} relationship in sub-threshold regime. This range is the drift-limited regime associated with deep trap states, similar to amorphous Si TFTs [84]. A methodology to properly consider this conduction regime (with its unique characteristics) in the extraction of the DOS is needed for polymer FETs.

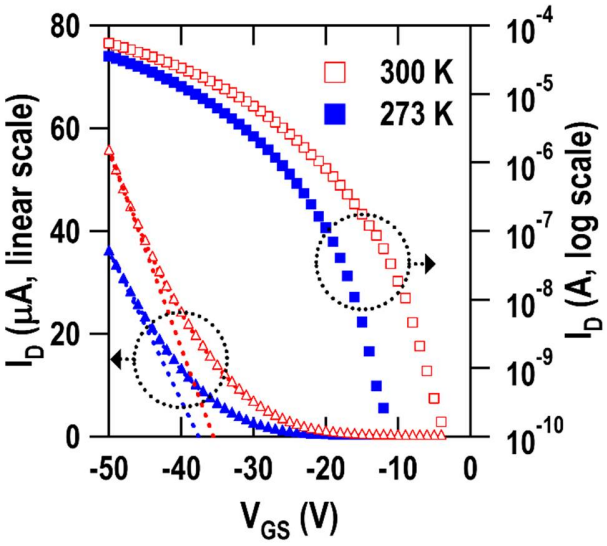

Figure 2.2: The transfer characteristics of PDPP-TVT FET at 300 K (opened) and 273 K (filled). Right axis: I_D in log scale (squares). Left axis: I_D in linear scale (triangles). Dotted lines indicate threshold voltage (V_T) of FET at each temperatures.

In the above threshold region, the slope of the log (I_D) vs. log (V_G) curve is expected to be 1, since the drain current varies linearly with gate voltage. In the sub-threshold drift-limited region the current voltage characteristics are given by (eq 1.6). These are illustrated in Figure 2.3 for two different temperatures. Figure 2.3(a) shows the log ($V_{GS} - V_{FB}$) dependent log (I_D) in sub-threshold regime. The turn-on voltage is used as a V_{FB}, where the sign of ($\Delta I_D/\Delta V_{GS}$) is changed. The dependence of log ($V_{GS} - V_T$) on log (I_D) in the above threshold regime is also shown in Figure 2.3(b). It is obvious that the slopes in each regime, which indicate the power law factor in the FET drain current equation, are greatly different. From Figure 2.3(a), the drift-limited power law factors for 300 K and 273 K were 4.63 and 3.65, respectively. In addition, from Figure 2.3(b), the above threshold regime power law factors for 300 K and 273 K were 1.04 and 1.10, respectively. The slope in the above

threshold regime was very close to unity, which means that the FET operated in the linear region. However, the drift-limited regime power law factor was much larger than its counterpart of the above threshold regime, which indicates not only the existence of a substantial number of deep trap states, but also the necessity of a different mobility calculation method for the drift-limited regime, rather than the conventional linear field-effect mobility extraction.

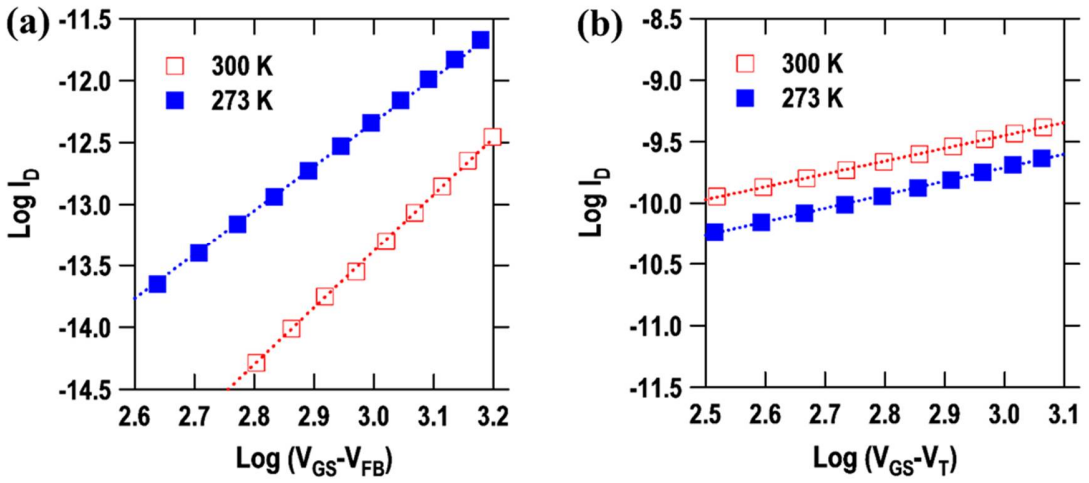

Figure 2.3: (a) log (I_D) vs. log (V_{GS}-V_{FB}) of PDPP-TVT FET in sub-threshold regime at 300 K and 273 K. b) log (I_D) vs. log (V_{GS}-V_T) of PDPP-TVT FET in above-threshold regime at 300 K and 273 K.

2.3.2 Density of States

To more accurately determine both activation energy and density of deep trap states, a composite mobility vs. gate voltage characteristic that spans both the sub-threshold and above threshold regimes is created. These regime have different current voltage characteristics: for the linear region, the field-effect mobility is described by (eq 2.1) over the full operating range.

$$\mu_{\mathrm{FET,Linear}} = \frac{\left(\partial I_{\mathrm{D}} / \partial V_{\mathrm{GS}}\right)}{\left(W/L\right) C_{\mathrm{i}} V_{\mathrm{DS}}} \qquad \text{(eq 2.1)}$$

This set of values is used for the calculation of activation energy in previous works [80-82]. It is called as a linear model in the remainder of this chapter.

In the drift-limited mobility regime, the current voltage characteristics are given by (eq 1.6). β is defined to satisfy the continuous transition of mobility at $V_{\mathrm{GS}} = V_{\mathrm{T}}$. This method of analysis of the sub-threshold drift-limited region has been employed by Nathan et al. [49]. This mobility model is referred to as the linear/drift model hereafter. The results of calculated mobility values based on the two models are shown in Figure 2.4(a).

In high mobility polymer FETs, the principal charge transport mechanism is MTR, as mentioned in Chapter 1.1.1 [35, 85]. According to the MTR model, the activation energy (E_{A}) can be calculated from the field-effect mobility, as described in (eq 1.1). From the activation energy data, it is possible to calculate the density of trap states based on Lang's method [77]:

$$N\left(E\right) = \frac{C_{\mathrm{i}}}{qa}\left[\frac{\partial E_{\mathrm{A}}}{\partial \left|V_{\mathrm{GS}}\right|}\right]^{-1} \qquad \text{(eq 2.3)}$$

where q is the elementary charge and a is a gate voltage independent effective accumulation layer thickness. In this case, a = 10 nm is used.

The calculated activation energy and the density of trap states based on the linear and linear/drift model are shown in Figure 2.4(b) and (c), respectively. For the activation energies in the sub-threshold regime, the linear model gives smaller values than the linear/drift model. In addition, there are some points where the slope is unnaturally in the linear model case. This difference in activation energy translates to a more significant change in the density of trap states. Contrary to the continuous curve of the linear/drift model calculation, the linear model results in a hump, which is an artifact. Such features may convey the impression that there is a local peak in the density of states, leading possibly to erroneous interpretations of charge transport data. There is a significant difference in the magnitude of the density of states calculated by the two methods for a wide range of energies. Previous work on sub-threshold behavior in FETs did not include the calculation of the density of trap states. The approach demonstrated in this chapter is very suitable for use in analyzing FET data for a number of disordered semiconductors.

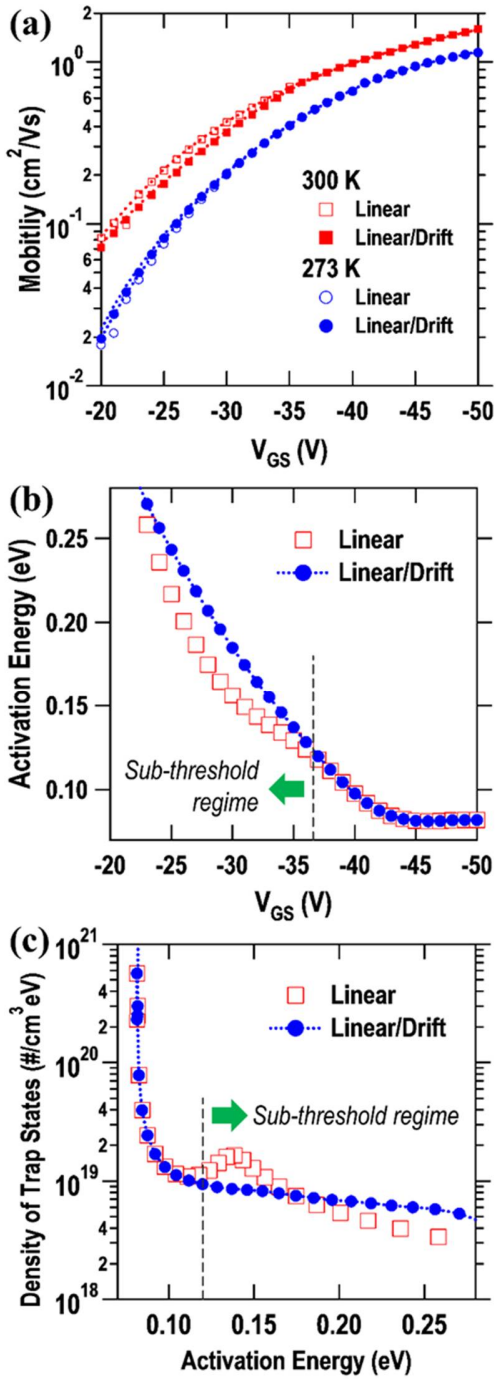

Figure 2.4: (a) Two field-effect mobility models of PDPP-TVT FET at 300 K and 273 K. (b) The activation energy of PDPP-TVT FET from two mobility models. (c) Density of trap states of PDPP-TVT based on the activation energy from two mobility models.

2.4 CONCLUSION

In summary, a method of calculating the density of trap states in a disordered semiconductor FET has been demonstrated in this chapter. This approach combines sub-threshold drift-limited region operation and above threshold operation to yield an accurate, artifact-free density of states profile. The density of states profile is extracted from the mobility versus gate voltage characteristic that extends from the above threshold region into the sub-threshold drift region. The method is demonstrated by analyzing data from PDPP-TVT FET. Such methods of analysis are inherently better suited for disordered and polycrystalline semiconductor based FETs and can also be used for single crystal FETs.

Chapter 3. Charge Transport Mechanism in Polymer FET*

3.1 INTRODUCTION

As mentioned in Chapter 1.1.2, polymer FETs generally have a wide sub-threshold regime due to a lot of disorder. Most of previous reports on charge transport in polymers transistors have focused exclusively on above threshold characteristics. Charge transport in deep states of polymer transistors has not been explored due to the difficulty in measuring the field-effect mobility in the sub-threshold region. The ability to characterize charge transport across a large range of carrier densities, including in the sub-threshold region, provides us with the best insights into charge transport phenomena in polymeric FETs.

In this chapter, charge transport mechanism in polymer FETs including deep states is analyzed and discussed based on sub-threshold regime modeling method which is described in Chapter 2.

* This chapter is based on Reference [50] S. Kim, T.-J. Ha, P. Sonar, and A. Dodabalapur, "Charge Transport in Deep and Shallow States in a High-Mobility Polymer FET," *IEEE Transactions on Electron Devices,* vol. 63, pp. 1254-1259, 2016. S.K. and A.D. conceived the idea and designed the experiments. T.-J.H. carried out fabrication of the device. P.S. synthesized the polymer. S.K. carried out characterization of devices and analyzed data.

3.2 EXPERIMENTAL

A polymer FET made with furan-flanked diketopyrrolopyrrole (DPP) with thienylene-vinylene-thienylene (PDPPFC24-TVT) is investigated, which has been reported as a high field-effect mobility polymer [16]. Figure 3.1 shows a chemical structure of PDPPFC24-TVT and a schematic structure of such a FET. N-doped silicon was used as gate, with 290 nm thermally grown SiO_2 dielectric layer on it. The dielectric layer gave the value of $C_i = 12$ nF/cm^2. The Ti/Au (2.5 nm/45 nm) source/drain electrodes were deposited on dielectric by thermal evaporation, and treated with self-assembled monolayer (SAM) of pentafluorobenzenethiol (PFBT). PDPPFC24-TVT film was spin coated and annealed under an inert atmosphere at 200˚C for 30 min. The temperature dependent measurement was done by a semiconductor parameter analyzer in a cryogenic probe station. A channel width and length of FET is 1000 μm and 50 μm, respectively.

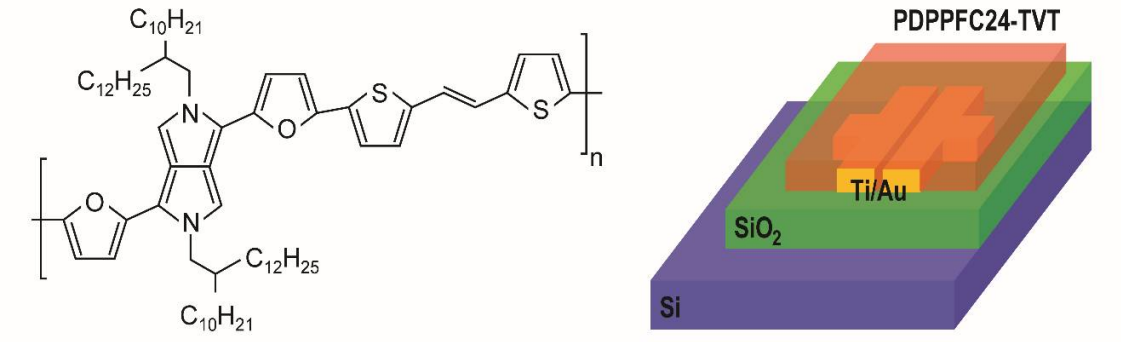

Figure 3.1: Chemical structure of PDPPFC24-TVT (left) and schematic of PDPPFC24-TVT FET (right).

3.3 RESULT AND DISCUSSION

3.3.1 Modeling

In addition to sub-threshold modeling technique explained in Chapter 1.1.2 and Chapter 2, above threshold and total current equations are needed for complete modeling. The linear region drain-source current in the above threshold regime can be described in similar way to the drift-limited current as follows (eq 3.1) [49, 50]:

$$\begin{aligned} I_{\mathrm{D,Above}} &\approx \mu_{\mathrm{FET,Above}} \frac{W}{L} C_{\mathrm{i}} \left|V_{\mathrm{GS}} - V_{\mathrm{T}}\right| \left|V_{\mathrm{DS}}\right| \\ &= \beta_{\mathrm{Above}} \frac{W}{L} C_{\mathrm{i}} \left|V_{\mathrm{GS}} - V_{\mathrm{T}}\right|^{\alpha_{\mathrm{a}}+1} \left|V_{\mathrm{DS}}\right| \end{aligned} \qquad \text{(eq 3.1)}$$

where V_{T} is the threshold voltage, $\mu_{\mathrm{FET,Above}}$ is the above threshold regime field-effect mobility, α_{a} is a power law factor, and β_{Above} is a pre-factor for the above threshold regime mobility. Typically α_{a} is close to 0, and when α_{a} is close to 0, (eq 3.1) represents the conventional linear region operation of a field-effect transistor.

Using (eq 1.5) and (eq 1.6), the total sub-threshold current by combining the diffusion/drift-limited current can be calculated as shown in (eq 3.2). Similarly, by combining (eq 3.1) and (eq 3.2), the total drain current can be described as (eq 3.3) [49, 50]:

$$\begin{aligned} I_{\mathrm{D,Sub}} = I_{\mathrm{D,Sub,Diff}} & \frac{1+\tanh\left(A\left(V_{\mathrm{GS}} - V_{\mathrm{A}}\right)\right)}{2} \\ + I_{\mathrm{D,Sub,Drift}} & \frac{1-\tanh\left(A\left(V_{\mathrm{GS}} - V_{\mathrm{A}}\right)\right)}{2} \end{aligned} \qquad \text{(eq 3.2)}$$

$$I_{D,Total} = I_{D,Sub}\frac{1+\tanh\left(B\left(V_{GS}-V_{B}\right)\right)}{2} + I_{D,Above}\frac{1-\tanh\left(B\left(V_{GS}-V_{B}\right)\right)}{2} \quad \text{(eq 3.3)}$$

where A, V_A and B, V_B are parameters for a smooth transition from the diffusion-limited to drift-limited regime and sub-threshold to above threshold regime, respectively.

Figure 3.2(a) shows a linear scale transfer curve of PDPPFC24-TVT FET and extraction of V_T to separate sub-threshold and above threshold regions, with V_{DS} = -10 V which means that FET operates in the linear region. Figure 3.2(b) and (c) show the measured transfer characteristics below and above threshold along with fits to diffusion-/drift-limited sub-threshold conduction and above-threshold conduction. Above-threshold conduction is modeled by well-known expressions for FET behavior in the linear regions as (eq 3.1) [22, 24], while below threshold is modeled by a similar approach that used for amorphous silicon FETs, by applying (eq 1.5) and (eq 1.6) [49, 50, 84]. It is immediately obvious that the sub-threshold regime extends over a large range of gate voltages and that above-threshold equations, which have hitherto exclusively been used to study transport in polymer FETs, are unable to model device operation until the gate voltage exceeds about 50 V. The fully modeled transfer characteristics for all operating temperatures are given in Figure 3.2(d). All modeling parameters are given in the Table 3.1.

Parameters	300 K	217 K	181 K	150 K	120 K	98 K
V_{FB} [V]	-16.5	-22.5	-26.0	-29.0	-33.5	-36.0
V_T [V]	-44.0	-47.7	-48.4	-49.4	-51.1	-51.8
I_{Off} [nA]	1.2	1.5	1.4	1.2	1.5	1.5
D_{it} [10^{12} $eV^{-1}cm^{-2}$]	4.8	6.6	7.9	14	18	25
α_d	3.04	2.69	2.75	2.88	2.49	2.46
α_a	0.01	0.01	0.04	0.02	0.03	0.04
V_A [V]	-24.5	-28.0	-31.0	-38.0	-40.5	-43.5
A	0.7					
V_B [V]	-48.0	-51.7	-52.4	-53.4	-55.1	-55.8
B	0.25					

Table 3.1: Modeling Parameters for PDPPFC24-TVT FET.

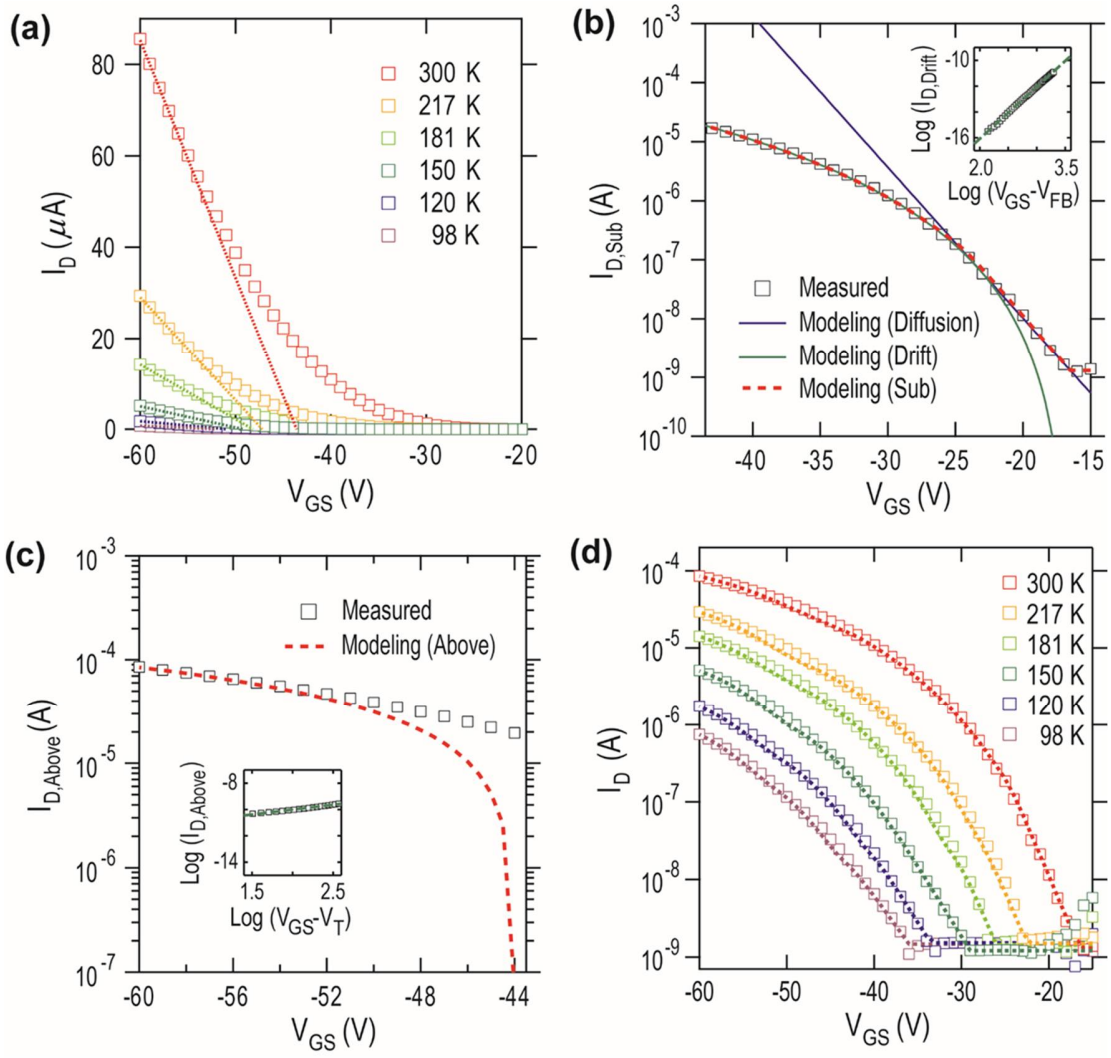

Figure 3.2: (a) Linear scale transfer curves of PDPPFCC24-TVT FET at 98 - 300 K. (b-c) Measured and modeled transfer curves of PDPPFC24-TVT FET at 300 K, for sub-threshold regime (b) and above threshold regime (c). Insets are showing the extraction of the power-law term from the slope of log I_D – log V_{GS} plot, for drift-limited regime (b) and above threshold regime (c), respectively. (d) Measured and modeled transfer curves of PDPPFC24-TVT FET at 98 - 300 K.

3.3.2 Conduction Regimes and Density of States

Figure 3.3(a) quantitatively summarizes the various regimes of conduction and their temperature dependence. It may be noticed that V_{FB} (V_{ON}) decreases in magnitude with increasing temperature [37]. It is also observed that the threshold voltage magnitude is reduced with increasing temperature. This is a very common characteristic of many thin-film transistors and is related to the shift in the flat-band voltage.

Also shown in Figure 3.3(a) is the transition from diffusion-limited sub-threshold conduction to drift-limited sub-threshold conduction. The drift-limited sub-threshold conduction regime grows at the expense of the diffusion-limited sub-threshold regime as temperature increases. This can be understood from density of trap states information. From modeling result, Figure 3.2(d), the mobility values above ($\mu_{FET,Above}$) and below ($\mu_{FET,Drift}$) the threshold voltage can be calculated as shown in Figure 3.3(b). Based on modeled mobility, the accurate activation energy and density of trap states information can be calculated, as shown in Figure 3.4 [72, 80]. The horizontal dashed lines in Figure 3.4 represent where the bulk trap density exceeds the interface trap density. Figure 3.4 will help us understand the transitions as a function of temperature and carrier density (i.e., gate voltage).

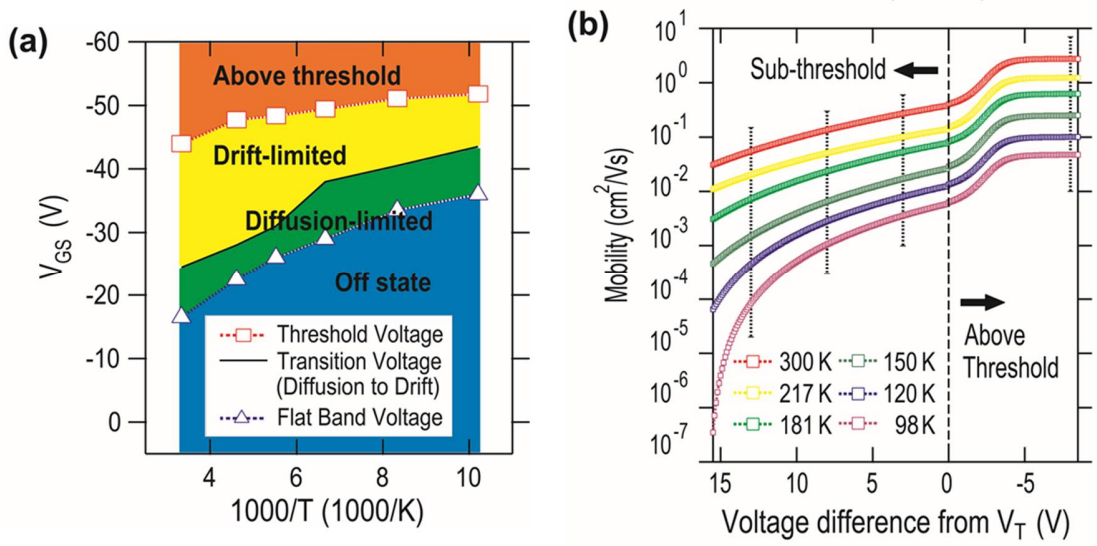

Figure 3.3: (a) Separation of operating regimes depends on temperature and gate voltage in PDPPFC24-TVT FET. (b) Modeled mobility of PDPPFC24-TVT FET at 98 - 300 K. Dotted lines indicate mobility extracting points; deep sub-threshold (13 V from V_T), mid sub-threshold (8 V from V_T), shallow sub-threshold (3 V from V_T) and above threshold (-8 V from V_T).

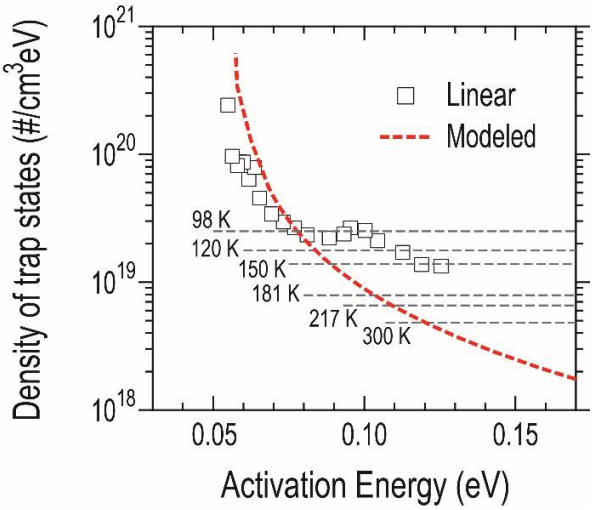

Figure 3.4: Density of trap states and the interface trap density at various operating temperatures (horizontal lines) of PDPPFC24-TVT FET.

3.3.3 Charge Transport in High-mobility Polymer FET

The mobility values are extracted at the specific gate voltages as indicated with vertical dashed lines in Figure 3.3(b). It is avoided that analyzing data close to the threshold voltage because the mobility extraction near threshold is prone to errors as both the above and below threshold equations predict different behavior. Accordingly, only voltages are considered that are well within the sub-threshold drift region and also gate voltages that are well above threshold. The mobility data are plotted in Figure 3.5(a-c). In Figure 3.5(a), the x-axis is in units of reciprocal temperature (T^{-1}) which is convenient for observing Arrhenius type behavior that is characteristic of MTR transport, as noted in (eq 1.1) [35, 36]. In Figure 3.5(b), the y-axis is mobility times $T^{1.5}$ and the x-axis is in units of $T^{-0.25}$, which is convenient for observing if VRH is present, as noted in (eq 1.3) [35, 38-41]. In Figure 3.6(c), the mobility is plotted as a function of T^{-2} which is to facilitate the observation of compliance with the GDM of Bässler and coworkers, as noted in (eq 1.4) [42-45]. All extracted parameters are shown in Table 3.2.

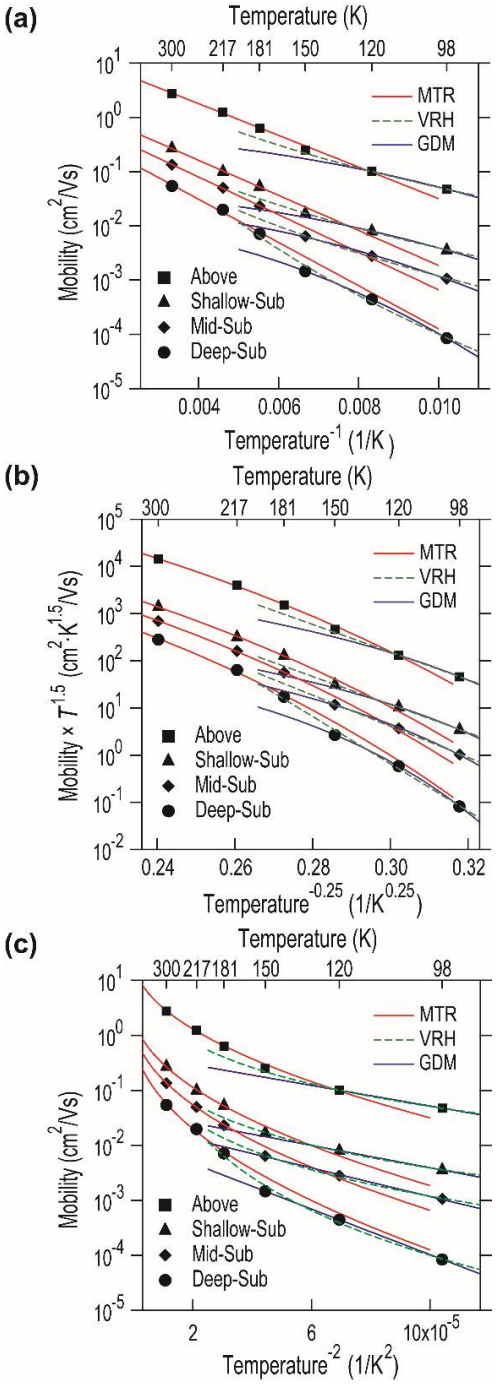

Figure 3.5: Temperature dependent mobility variation of PDPPFC24-TVT FET along with T^{-1} (a), $T^{-0.25}$ (and mobility times $T^{1.5}$ for y-axis) (b) and T^{-2} (c). Red solid, green dotted and blue solid lines represent the fitted result of MTR, VRH and GDM, respectively.

Parameters	Above Threshold	Shallow Sub-Threshold	Mid Sub-Threshold	Deep Sub-Threshold
$\mu_{0,MTR}$ [cm^2/Vs]	26.4	3.18	1.94	1.21
E_A [eV]	0.058	0.064	0.069	0.079
$D^{0.25}$ [$eV^{0.25}$]	7.0	6.6	7.4	11.1
$C(\sigma)^2$ [eV^2]	1.6×10^{-4}	1.7×10^{-4}	2.2×10^{-4}	3.5×10^{-4}

Table 3.2: Extracted parameters for MTR/VRH/GDM transport estimation from modeled mobility values.

Figure 3.5(a-c) taken together clearly show the following trends: At higher temperatures and at high carrier density, there is good agreement with the predictions of the MTR model. At low temperatures and at low carrier densities, MTR type transport is not observed; instead both the VRH and GDM models fit the data fairly well, with the VRH model being a slightly better fit. This data helps settle the question as to which transport models are best suited to describe charge transport in polymer transistors. Over the years, all three models have been used to fit FET mobility data from different semiconductor materials [8, 37, 41, 45, 86]. These fits all seemed to work for the respective materials that were considered. This data suggest that the three models are valid over specific ranges of carrier density and temperature. If the trap depths are very large relative to kT, as is the case at low temperatures and at low carrier densities, MTR is not a suitable model. This also is the case in low mobility and most amorphous polymer based FETs in which the trap depths are typically large. When the trap depths are large, both VRH and GDM fit the data fairly well. These models do not invoke a reference energy level – such as a band-edge. They are derived from the Miller-Abrahams type hopping [87], in which carriers hop between localized states. In the GDM, the density of trap states is a Gaussian whereas in VRH the density of states shape is not specified. It is helpful to think of both MTR and

hopping occurring simultaneously in this type of material, with one of them dominating under appropriate conditions.

It has been able to show the transition between hopping and MTR transport because of the availability of extracting mobility values at very low carrier densities – in the sub-threshold region. Polymer FETs have extensive sub-threshold regions which have not been considered in transport studies so far. In considering the sub-threshold regime as well as above threshold operation together, it is possible to get a unified picture of charge transport in high mobility polymer FETs. For extended state transport to be observed, the density of trap states must be lowered so that the Fermi level can reach band states. The trap density is lower in amorphous semiconductors materials and extended state transport has been observed in amorphous oxide semiconductors [88] and also evidence of disorder-free transport has been reported for amorphous polymers [48]. In crystalline polymers, extended state transport has not yet been reported, despite the impressive mobility values that have been achieved [89]. In future, it may be possible to realize low enough trap concentrations in such crystalline polymers to observe extended state transport [89]. This will require a synergy between molecular design, dielectric choice, and processing and crystallization conditions.

3.4 CONCLUSION

In summary, charge transport in trap states across a wide range of energies in PDPPFC24-TVT based FETs has been investigated. Both above threshold and sub-threshold regimes of operation are considered in analysis via modeling process. At low carrier densities and at low temperatures, charge transport is primarily by hopping. At higher carrier densities (including in the sub-threshold region) and at higher temperatures, the multiple trap and release model fits the data much better. It can be proposed that charges move by both MTR and hopping, with one of them dominating under appropriate conditions. The observation of this transition in transport behavior is possible as it is available to consider a wide range of carrier densities, including those that are below threshold. These results clarify and place in perspective the findings of many previous reports on charge transport in conjugated polymers.

Chapter 4. Polarization Effects on Charge Transport in Polymer FETs*

4.1 INTRODUCTION

As mentioned in Chapter 1.1.3, charge transport in polymer semiconductors is mostly polaronic in nature. From previous results, polar molecules in the dielectric layer and also in the ambient atmosphere have been demonstrated to enhance polarization effects which increases the binding energy of trapped charge carriers in polymer FETs [52, 53]. In this chapter, the polarization induced trapping enhancement by dipoles in the gate dielectric layer and ambient air are investigated *simultaneously* through the experiment with varying conditions of surface dielectric and polar analytes in atmosphere.

4.2 EXPERIMENTAL

The DPP-thienothiophene copolymer (PDPP2T-TT-OD, purchased from Sigma-Aldrich) is used as a semiconducting polymer layer. The chemical structure of PDPP2T-TT-OD and the device structure of the FETs are shown on Figure 4.1(a) and (b), respectively. N-doped silicon was used as gate. As the dielectric layer, ZrO_2 high-k layer is deposited first via solution processing as described in previous work [91]. The thickness of the ZrO_2 layer is about 90 nm. To lower the dielectric constant of the gate insulator in contact with the polymer semiconductor, a thin SiO_2 (10 nm) layer is deposited via Plasma-enhance chemical vapor deposition (PECVD). A ZrO_2-SiO_2 bilayer and an only high-k ZrO_2 monolayer dielectrics possess values of capacitance per unit area (C_i) of 134 and 220

* This chapter is based on Reference [90] S. Kim and A. Dodabalapur, "Polarization Effects from Ambient and Dielectric on Charge Transport in Polymer Field-effect Transistors," *Advanced Materials* (under review). S.K. and A.D. conceived the idea and designed the experiments. S.K. carried out fabrication, characterization of devices and analyzed data.

nF/cm^2, respectively. PDPP2T-TT-OD film was spin coated on octadecyltrichlorosilane (ODTS) self-assembled monolayer (SAM) treated surface and annealed under an inert atmosphere at 140˚C for 30 min. The Au (30 nm) source/drain electrodes were deposited on the polymer layer by thermal evaporation. The electrical characteristics of the FET were measured at 300 - 350 K, using a semiconductor parameter analyzer in a cryogenic probe station under N_2 and ethanol 2000 ppm atmosphere. The channel width (W) and length (L) of the FET is 1000 µm and 50 µm, respectively.

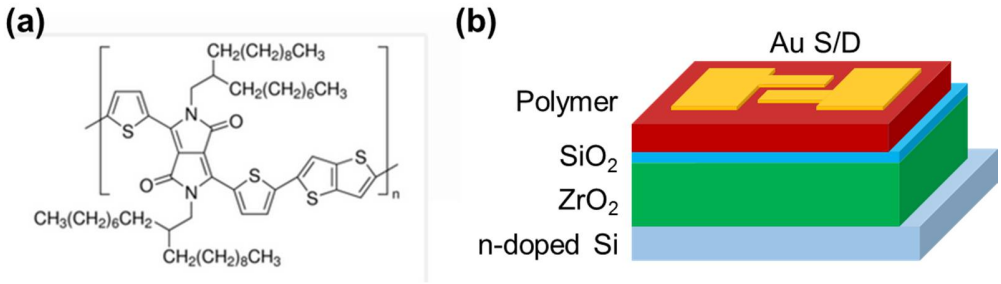

Figure 4.1: (a) The chemical structure of PDPP2T-TT-OD, (b) device structure of PDPP2T-TT-OD FETs.

4.3 RESULT AND DISCUSSION

4.3.1 Devices Characteristics

Figure 4.2 shows the transfer and output characteristics of PDPP2T-TT-OD FETs with bilayer and monolayer dielectrics under N_2 atmosphere. The range of applied gate voltage (V_{GS}) is 0 to -12 V and 0 to -8 V for bilayer and monolayer dielectric FETs, respectively. As we can expect based on previous reports, owing to weaker polarization

effects from the dielectric, low-*k* dielectric interfaces result in better electrical properties including smaller sub-threshold swing, smaller threshold voltage (V_T) and larger current flow [53].

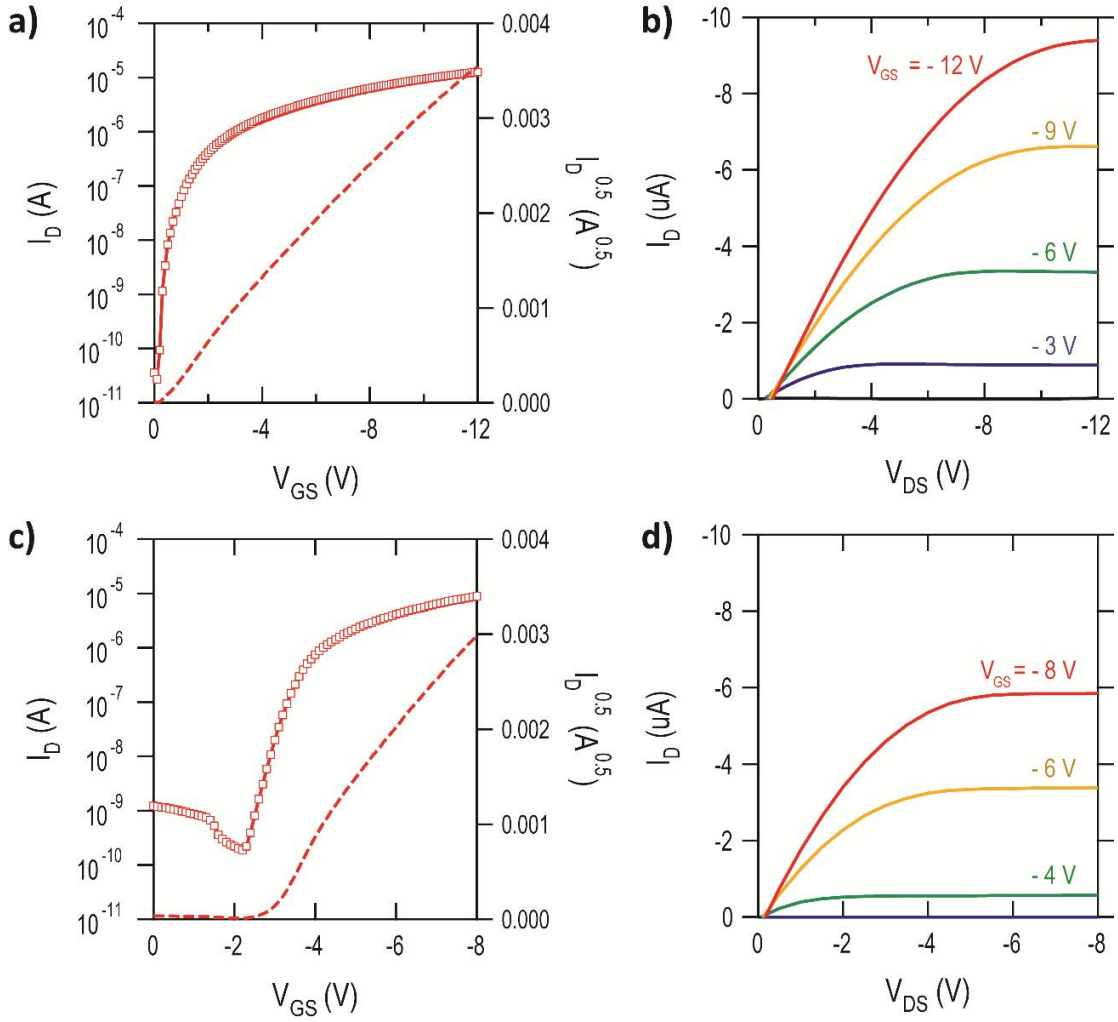

Figure 4.2: The transfer characteristics (a) and output characteristics (b) of PDPP2T-TT-OD FET with ZrO_2/SiO_2 bilayer dielectric, and the transfer characteristics (c) and output characteristics (d) of PDPP2T-TT-OD FET with ZrO_2 monolayer dielectric. For the transfer characteristics (a, c), the applied drain-source voltage (V_{DS}) is -12 V and -8 V, respectively.

4.3.2 Effect of Ethanol on Field-effect Mobility

Both types of devices are measured in N_2 and in nitrogen containing 2000 ppm ethanol ambients to determine the effect of polar analytes on the mobility of these FETs. Figure 4.3 shows the difference of drain current of PDPP2T-TT-OD FETs with bilayer and monolayer dielectrics under N_2 and ethanol-containing nitrogen atmosphere. The mobility of FETs decreased when exposed to ethanol atmosphere [52].

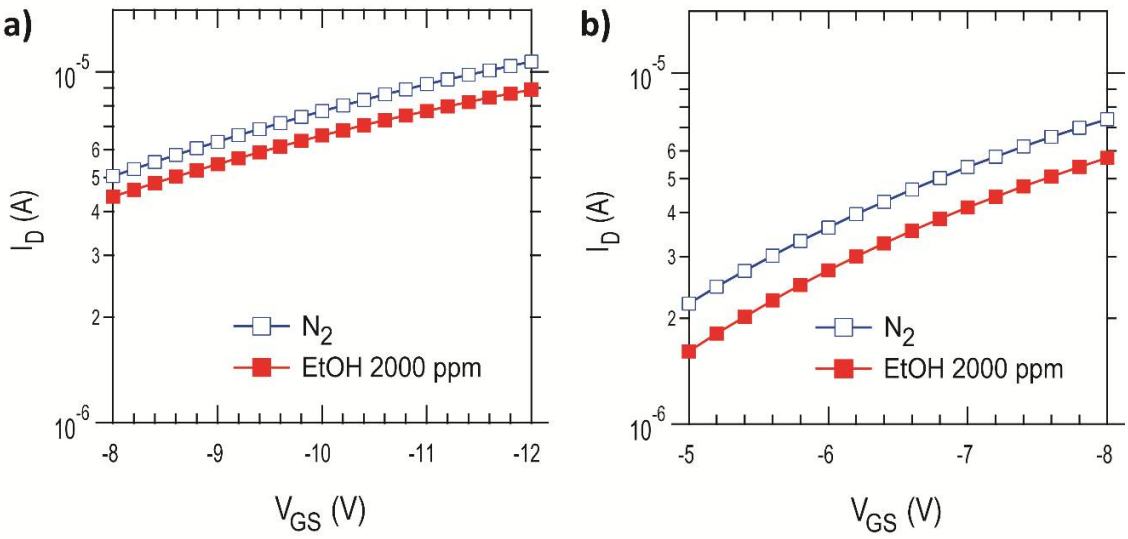

Figure 4.3: The transfer characteristics of PDPP2T-TT-OD FETs with ZrO_2/SiO_2 bilayer dielectric (a) and with ZrO_2 monolayer dielectric (b). The applied drain-source voltage (V_{DS}) is -12 V and -8 V, respectively.

4.3.3 Activation Energy Difference by Polar Analytes

As mentioned in chapter 1.1.1, it is possible to calculate charge carrier activation energy (E_A) from the field-effect mobility of FETs at different temperature, as shown in (eq 1.1). The temperature-dependent averaged mobility in the range of V_{GS} larger than V_T is plotted in Figure 4.4. For more accurate analysis, the mobility values are extracted from 5 devices for each structure. The measured temperature points are 300, 307, 315, 323, 332, 341 and 350 K. For the bilayer dielectric FETs, E_A is 55.1 meV in N_2 and 83.0 meV in ethanol 2000 ppm. For the monolayer dielectric FETs, E_A is 122 meV in N_2 and 150 meV in ethanol 2000 ppm. In contrast to E_A of the bilayer dielectric FETs, which is increased 50.6 %, E_A of the monolayer dielectric FETs is increased only 23.0 % in ethanol atmosphere, comparing to the E_A in N_2. This means that the activation energy, which is closely related to trap depth, is affected more by polar analytes for the bilayer dielectric FETs. It shows that the polarization effect of polar analytes in present in air is more severe for the device has a lower polarization effect from dielectric (i.e., the low-*k* dielectric interface device).

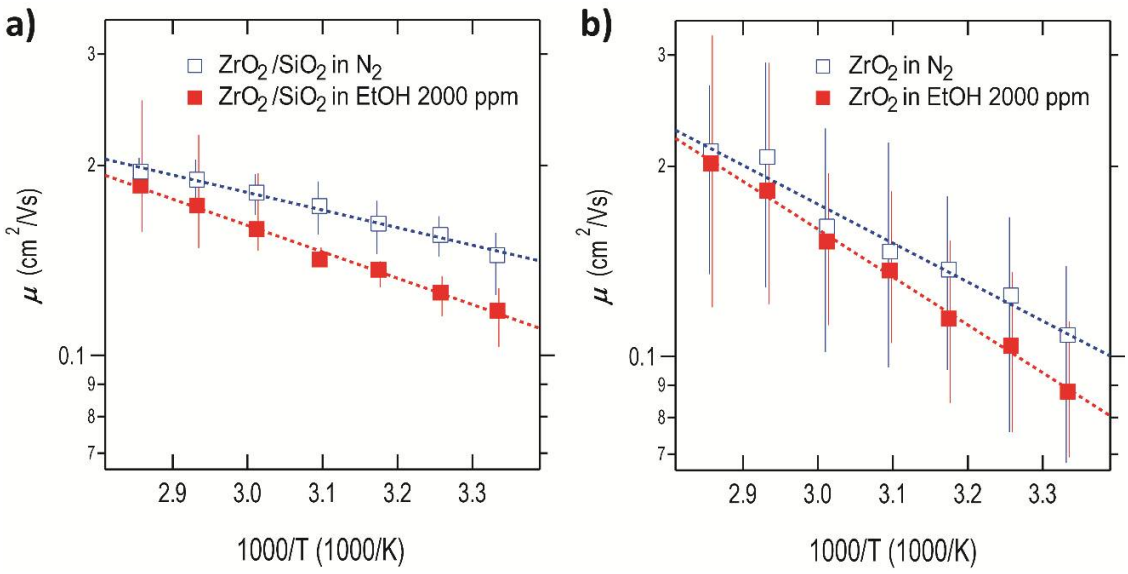

Figure 4.4: The temperature dependent mobility of PDPP2T-TT-OD FETs with ZrO_2/SiO_2 bilayer dielectric (a) and with ZrO_2 monolayer dielectric (b). Error bar shows the distribution of mobility for 5 devices.

4.3.4 Density of States

The density of states (DOS) of FETs can be calculated using a similar procedure to that used in Chapter 2 and 3. The extracted DOS of PDPP2T-TT-OD FETs with bilayer and monolayer dielectrics under N_2 and ethanol atmosphere are shown in Figure 4.5. First, it is clear that the bilayer dielectric device has lower activation energy than that of the monolayer dielectric device, which is well-correlated with previous reports and the transfer characteristics of FETs from Chapter 4.3.2 [53]. In addition, more interestingly, the DOS is affected by polar analytes especially in the region of lower activation energy (shallower states). From Figure 4.5, it would be quite reasonable to suggest that traps located near to band-like region behave like deeper traps due to the presence of polar analytes as

mentioned in Chapter 1.1.3 and Figure 1.9(b). In other words, polar anayltes enhance the trap depths.

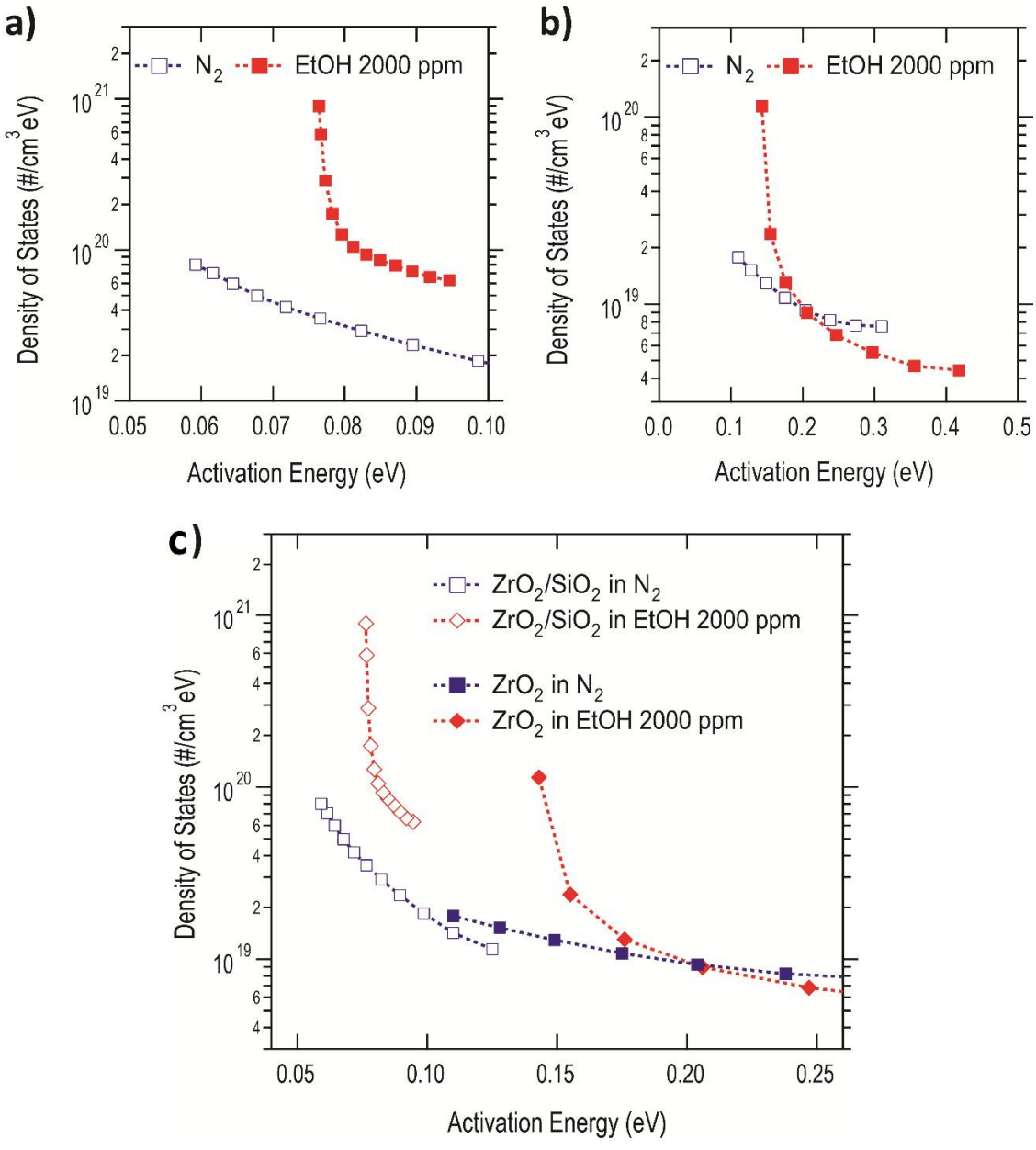

Figure 4.5: DOS of PDPP2T-TT-OD FETs with ZrO_2/SiO_2 bilayer dielectric (a), with ZrO_2 monolayer dielectric (b) and both devices on the same plot (c).

These results can be explained in the following way. From Chapter 4.3.2 and 4.3.3, dipoles present in air and in the gate dielectric basically enhance trap depth. It is clearly observed in these experiments that both dipoles in the ambient air and in the gate insulator influence the mobility by enhancing the trap depths of charge carriers. The effect of ambient dipoles is more marked when the gate insulator interface is less polar. When the gate insulator (near the interface with the semiconductor) is also very polar, then polar dipole containing ambients still enhance trap depths of charge carriers, but not to the same degree as in the case of a lower *k* interface.

These effects are also manifest in the calculated density of occupied states. Firstly, let us consider only the effect of a polar gate insulator on the density of states in the absence of polar vapor ambients. The effect of the polar gate dielectric is to lower the energy (increase the trap depth) of the occupied states. When polar vapor molecules are introduced into the ambient, the density of states increases substantially, particularly at lower activation energies. Thus polarization effects from the ambient affect the shallower trap states and not the very deep trap states.

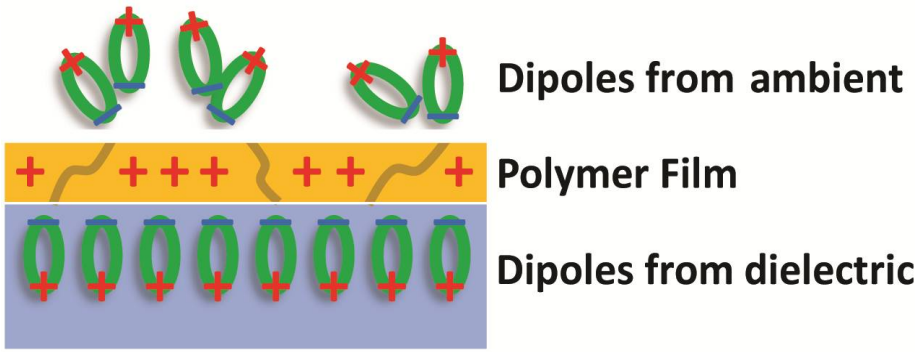

Figure 4.6: Visual description of polaronic effect of dipoles from air and dielectric on polymer FET.

4.4 CONCLUSION

In conclusion, a polarization effects of dipoles on charge transport in polymer FETs from dipoles in the gate dielectric and in ambient air are investigated in detail via an analysis of the characteristics of PDPP2T-TT-OD FETs with ZrO_2/SiO_2 bilayer dielectric and with ZrO_2 monolayer dielectric. From temperature dependent mobility data and the extracted DOS curve, the polarization effect from both dipoles in dielectric and air is confirmed. The polarization effects are most severe when individual effects from the ambient air and gate insulator are both present. When the gate insulator interface is very polar, the effects of dipoles in the ambient air is weaker than the case for a relatively non-polar dielectric-semiconductor interface.

Chapter 5. Polar Vapor Effect on Charge Transport in Graphene FET*

5.1 INTRODUCTION

There are several previous work have shown that the dielectric environment atop a graphene monolayer, including fluoropolymer, is a key factor for improved electrical properties of graphene FETs, as mentioned in Chapter 1.2.2 [60, 62, 63, 93, 94]. For better understanding of physics of fluoropolymer effect on graphene FETs, it has been investigated under polar vapor flow condition. While the discussion by A.K.M. Newaz, et al. of various dielectrics surrounding graphene included various effects unique to the liquid phase, including the formation of an electrical double layer and the ever-present charged ions in solution, we emphasize that our experiments do not involve device measurements in liquid media [94]. Indeed, in contrast to liquid-phase experiments, it was available to exert greater control over the extent to which the polar molecules and bonds of fluoropolymer thin films organize atop the graphene via annealing experiments. Both the charged impurity neutralization by molecular dipoles and dielectric environment modification aspects of the hypothesis directly influence the aforementioned electrical characteristics of a graphene FET, and will be discussed in this chapter.

However, the chemical and structural complexities of the fluoropolymer film/graphene system, which include variables such as the degree and orientation of polarization interactions between graphene and the C–F fluoropolymer bonds, complicate the precise identification of the physical phenomena involved in the observed electrical

* This chapter is based on Reference [92] B. C. Worley, S. Kim, S. Park, P. J. Rossky, D. Akinwande, and A. Dodabalapur, "Dramatic vapor-phase modulation of the characteristics of graphene field-effect transistors," *Physical Chemistry Chemical Physics,* vol. 17, pp. 18426-18430, 2015. B.C.W., S.K. and A.D. conceived the idea and designed the experiments. S.K. and S.P. carried out fabrication and characterization of devices. S.K. analyzed data. B.C.W. and S.K. contributed equally.

improvements. Thus, vapor phase molecules are very helpful in studying trapping and transport phenomena and help clarify the chemical physics of the system.

5.2 EXPERIMENTAL

Device fabrication begins with monolayer graphene grown via chemical vapor deposition on copper foil [95]. Next, poly(methylmethacrylate) is used to transfer a square centimeter-sized piece of graphene onto thermally-grown SiO_2 (285 nm thick, on heavily-doped Si wafer) via a wet transfer method described in previous work [95, 96]. Oxygen plasma reactive ion etching was used to define the active channel region to ensure device isolation as shown in Figure 5.1. Source and drain contacts were patterned by e-beam lithography to give a channel W/L of 60/1 μm. Ti/Pd (3/50 nm) contacts were e-beam evaporated to complete the top contact, bottom gate graphene FET. Figure 5.1(a) shows a cross-sectional schematic of the completed graphene FET. A basic experimental setup for ambient, room temperature testing of graphene FET devices under exposure to various polar solvent vapors is shown in Figure 5.1(b). After saturating a piece of filter paper with a few drops of the desired reagent-grade liquid solvent, the paper was rolled and placed it in a syringe. This syringe is connected to a nitrogen gas line, and pressure is supplied by a peristaltic pump with variable flow rates. The tip of the syringe is placed within close proximity to the graphene FET channel surface, where the graphene FET is secured atop the vacuum chuck of a Cascade probe station, which is open to the air. Electrical characterization is carried out with a semiconductor parameter analyzer.

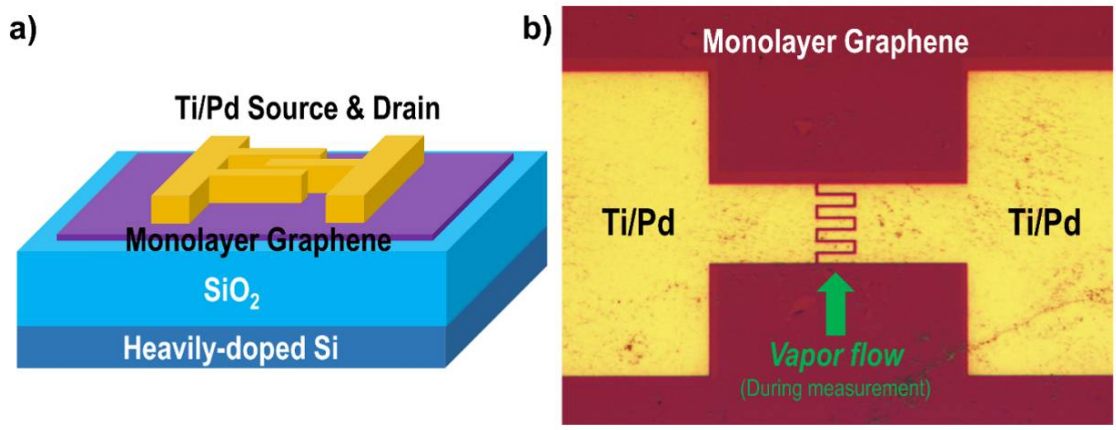

Figure 5.1: Schematic cross-section (a) and optical image (b) of graphene FET device, showing the channel area and the introduction of polar vapors.

5.3 Result and Discussion

5.3.1 Effect of Dipole Moment of Polar Vapor Molecules

The electrical characteristics of our graphene FET in ambient, along with normalized results for exposure to nitrogen, isopropyl alcohol (IPA), ethanol, and acetone vapors are shown in Figure 5.2(a). Initially, the Dirac peak of the as-fabricated graphene FET is observed at around +40 V, primarily due to adventitious doping of graphene by charged impurities and defects [57]. Figure 5.2(b) shows a clear relation between dipole moment of impingent polar vapor molecule and resultant Dirac voltage shift. Dipole moment data for the vapors used in the experiment were obtained from 'Selected Values of Electric Dipole Moments for Molecules in the Gas Phase' [97]. It was determined that the chemical property which best explains the results of experiments is dipole moment. Figure 5.2(c) displays initial graphene FET values of both hole (a) and electron (b) mobility of 748 and 649 cm^2/Vs, respectively. Note that the initial mobility values are rather low due to the significant presence and large possible variety of charged impurities and defects

present in and around the graphene layer of samples. Also shown is the initial carrier concentration of $6.21 \cdot 10^{11} cm^{-2}$ (Figure 5.2(d)). The fitting model described by S. Kim et al. was used to calculate both μ and N_0 [98]. Figure 5.2(a) shows that the exposure of a graphene FET to various polar analyte vapors results in a significant shift in the Dirac voltage toward zero. Figure 5.2(b) illustrates the dependence of the down shift in the Dirac voltage on the magnitude of the dipole moment of impingent analyte type. Both IPA and ethanol have roughly the same dipole moment, while acetone is significantly more polar. These changes are consistent with nearly complete neutralization or screening of charged impurities and defects by electrostatic or van Der Waals interaction with the polar analytes used. On the other hand, Figure 5.2 and 5.3 illustrate that molecules with little to no dipole moment, such as nitrogen (N_2) and hexane, have little to no observable effect on measured device characteristics. While data shown in Figure 5.3 was measured on a different device than that in Figure 5.2, it supports the hypothesis that the dipole moment of impingent vapor molecules is the distinguishing factor for improvement of graphene FET device characteristics. The graphene mobility values are observed to increase with increasing dipole moment of impingent solvent molecule. These results are shown alongside the initial mobility in Figure 5.2(c). Simultaneously, N_0 is observed to decrease with increasing dipole moment. As discussed below, mobility and carrier concentration are directly influenced by charged impurities.

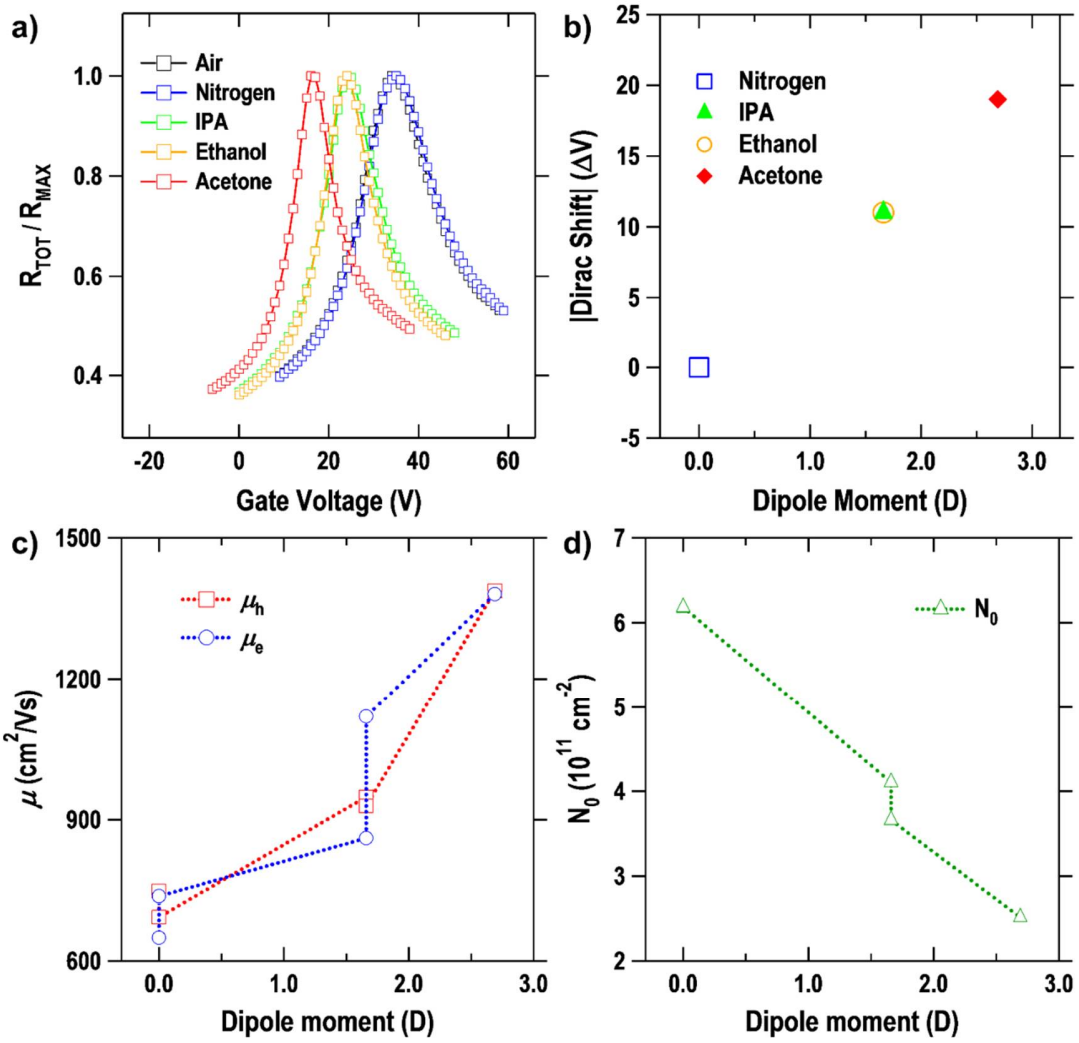

Figure 5.2: Plot of normalized resistance as a function of gate voltage for a graphene FET in ambient under various analyte exposure conditions (a). Plot of Dirac shift (b), electron and hole mobility (c), and residual carrier concentration (d) as a function of dipole moment of each analyte vapor.

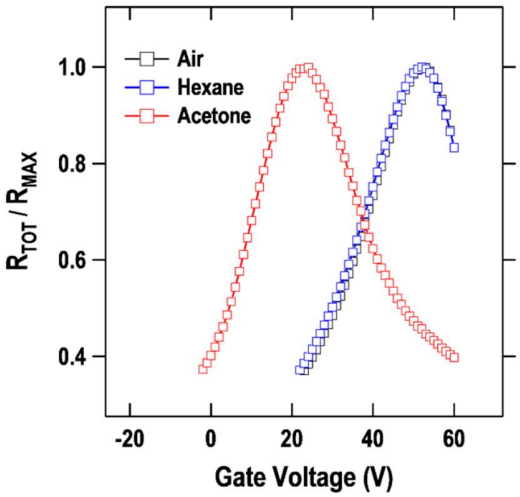

Figure 5.3: Plot of normalized resistance as a function of gate voltage for a graphene FET (different than device for Figure 5.2) in ambient under various analyte exposure conditions, including hexane exposure.

5.3.2 Reversibility

In a display of reversibility remarkably similar to that seen in previous work on fluoropolymer coatings, Figure 5.4 shows that, after turning off the flow of acetone vapor, the Dirac voltage begins to shift back towards the positive value observed before polar analyte exposure. This behavior is consistent with the hypothesis that, after the flow of acetone to the graphene has stopped, acetone molecules previously adsorbed to the graphene surface gradually desorb as time passes, and cease to screen or neutralize the fields from charged defects. In comparison to acetone, other polar molecules would have varying rates of desorption from the defect and impurity sites in graphene. This would be a diffusion-limited or electric field dependent behavior. Thus, the electric fields of charged impurities and defects may again act to scatter charge carriers, and this is observed in the form of increasingly positive Dirac voltage shifts (Figure 5.4(b)), reduced mobility (Figure

5.4(c)), and increased carrier concentration (Figure 5.4(d)). Nitrogen is shown to cause no significant shift in the measured graphene FET electrical characteristics. The apparent reversibility of the interaction between polar molecules and graphene indicates that the nature of this phenomenon is not one of electron transfer, but rather one of charge-screening or neutralization of charged impurities. The reversible charge-screening or neutralization effects of polar vapors are analogous to those brought about by the application and subsequent removal of a fluoropolymer thin film on graphene observed in previous works [62, 63].

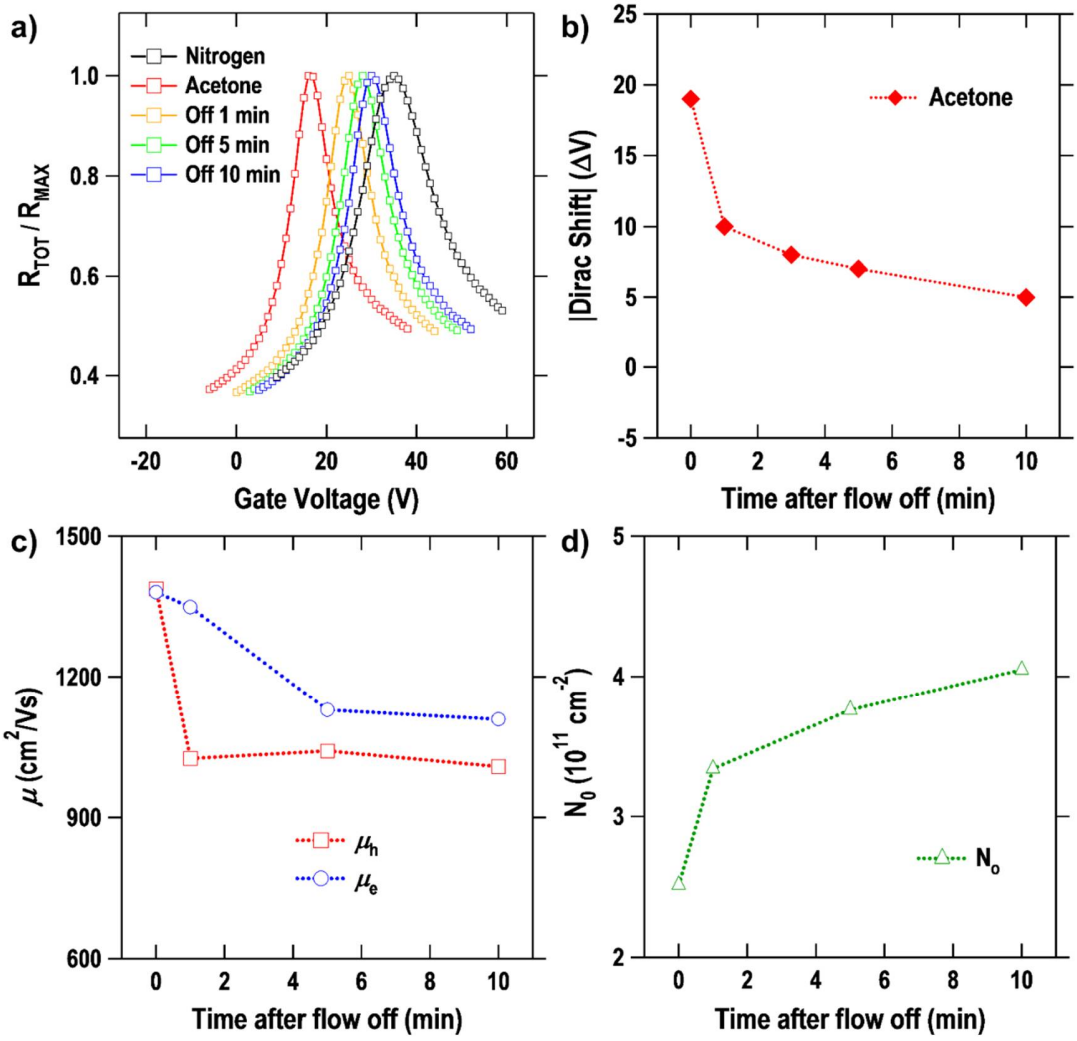

Figure 5.4: Plot of normalized resistance as a function of gate voltage showing return of Dirac peak to original position over time after stopping exposure to acetone vapor (a). Plot of Dirac shift magnitude (b), electron and hole mobility (c), and residual carrier concentration (d) as a function of total elapsed time after acetone vapor flow was stopped.

5.3.3 Discussion on Experimental Results

It is possible that the vapor-phase acetone molecules form a non-uniform layer atop the graphene, self-organizing into an inhomogeneous dielectric layer under the influence of the electric field generated by charged impurities and defects so as to neutralize the charged impurities via electrostatic interaction. The present experiment does not provide insight on such a detailed extent of characterization, because we conducted these experiments in ambient air. Nevertheless, forming a much higher-*k* dielectric environment than that made up by the now displaced ambient air, the acetone layer decreases the dimensionless coupling constant a as discussed by C. Jang et al. [60]. Others have also postulated that high-*k* dielectrics could play a role in screening Coulombic impurity scattering. Again, the simple but paramount difference in phase of media (liquid versus vapor) used to modify the graphene environment between these experiments and those described in A.K.M. Newaz, et al. [94]. The evidence for impurity neutralization is, however, very clear. As mentioned above, the present vapor-phase experimental design is a simpler system than the fluoropolymer thin-film-capped graphene FET reported previously. Instead of the multitude of C–F bonds oriented first, along the fluoropolymer backbone, and second, according to reorganization of the thin film during annealing, vapor phase molecules from analytes of high purity (99%+) and known dipole moment are expected to be free to adopt the optimal conformation atop the graphene so as to affect the greatest extent of charged impurity neutralization at room temperature (annealing being unnecessary). Additionally, “in situ” changes in relative local concentration/dissipation of polar analyte molecules from the graphene surface can be observed in real time, unlike the fluoropolymer capping method, which requires separate processes to deposit and remove the thin film. It should be noted, however, that the fluoropolymer capping method does hold great potential as a practical method for mitigating thee detrimental effects of charged

impurities on graphene transistors, and has also been shown to improve the reliability and operating lifetime of graphene FETs [30, 65].

The clarity of vapor-phase experimental results, supported by strong agreement with data gathered from previous work, affords strong evidence that the simple act of bringing polar molecules into contact with graphene and possibly other 2-D materials can act to improve the electrical characteristics of the system by their electrostatic or van Der Waals interaction with charged impurities and defects. The two principal mechanisms by which charged impurities affect graphene transport, long- and short-range scattering, are pivotal in understanding our experimental results. Long-range scattering of charge carriers by impurities is the dominant mechanism limiting mobility in graphene at high carrier concentrations. Polar vapors evidently act to screen the Coulombic interaction between charged impurities and carriers, mitigating long-range scattering [58, 60, 99]. Simultaneously, polar vapors decrease both the minimum conductivity and, N_0, which are determined by short-range scattering [56, 60, 62].

5.4 CONCLUSION

In conclusion, it has been shown that polar vapors delivered to graphene FETs result in favorable changes to the Dirac voltage, mobility, and residual carrier concentration. The magnitude of the Dirac voltage is greatly reduced, the mobility of both holes and electrons are increased, and the residual carrier concentration is decreased. The magnitude of these changes tracks with the dipole moment of vapor molecule used. These changes, along with their reversibility upon vapor molecule desorption, are analogous to previous work on graphene FETs coated with films of various polar fluoropolymers. The evidence strongly suggests that polar groups significantly screen the fields of charged impurities (but, do not transfer electrons), which improves mobility due to a reduction in charged impurity scattering. Alteration of the dielectric environment surrounding the graphene monolayer may also reduce the fine structure constant of graphene, contributing to the observed improvements.

Chapter 6. Graphene Nano-ribbon FET*

6.1 INTRODUCTION

As mentioned in Chapter 1.2.3, graphene nano-ribbons (GNRs) are been being investigated as they possess a non-zero bandgap in contrast to graphene sheets, which have zero bandgap [66, 101]. Therefore, GNRs might be more suitable as a channel material in FETs which requires a high on/off ratio. The other electrical properties of GNR FETs apart from on/off ratio, however, are not as good as those of corresponding graphene sheet FETs. Most GNR FETs have a larger hysteresis, a lower mobility and a larger Dirac voltage than those of graphene sheet FETs. The critical factor that results in degraded performance of GNR FET is edge defects, since GNR due to their geometry have a larger number of edges per active channel width. Moreover, edges of patterned GNR from chemical vapor deposition (CVD) grown graphene do not have a perfect chirality and inevitably have more broken bonds. Thus defect passivation or amelioration assumes considerable importance if the excellent potential of GNR as a semiconducting material is to be realized. In this chapter, the effect of polar vapors on the electrical characteristics of GNR FETs, which is fabricated via patterning from CVD grown graphene monolayer sheet, is discussed. An ultimate goal is to use these as model studies in designing suitable cap layers that both protect the nano-ribbons from the ambient and favorably influence, to a considerable degree, their electrical properties.

* This chapter is based on Reference [100] S. Kim, S. Park, D. Akinwande, and A. Dodabalapur, "Electrical performance enhancement of 20 nm scale graphene nanoribbon field-effect transistors with dipolar molecules," in *Device Research Conference (DRC), 2016 74th Annual*, 2016, pp. 1-2. S.K., S.P., D.A. and A.D. conceived the idea and designed the experiments. S.K. and S.P. carried out fabrication and characterization of devices. S.K. analyzed data.

6.2 EXPERIMENTAL

Monolayer graphene is grown via CVD on copper films. Following this, a square centimeter-sized piece of graphene is transferred onto thermally grown 90 nm-thick SiO_2 or 30 nm-thick HfO_2 which is grown via atomic layer deposition (ALD) on heavily doped Si substrate via a wet transfer method using poly(methyl methacrylate) (PMMA). Active GNR and graphene sheet channel is patterned bye-beam lithography and defined by oxygen plasma reactive ion etching. Finally, Ti/Pd source/drain contacts are patterned via e-beam lithography. Figure 6.1 shows the micrograph of uniformly patterned 20 nm width GNRs.

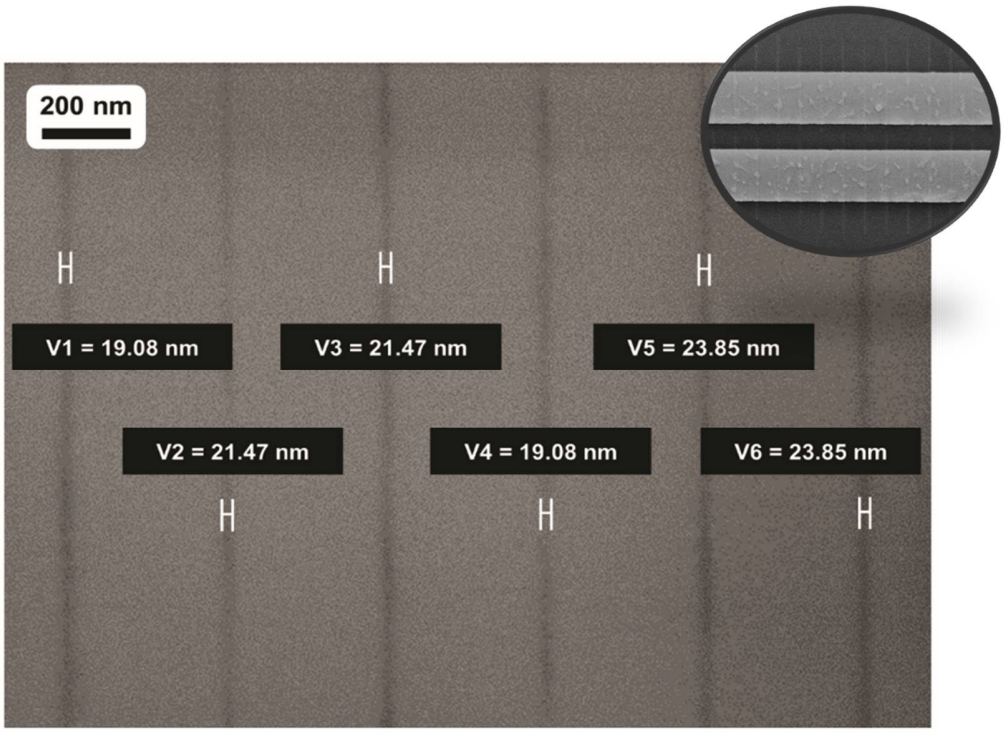

Figure 6.1: SEM image of 20 nm width GNRs patterned from CVD grown monolayer graphene sheet. Inset (right upper side) shows the image after S/D metal deposition.

6.3 RESULT AND DISCUSSION

6.3.1 Effect of Polar Molecules

The effect of polar molecules on electrical properties of GNR FETs has been investigated, with similar experimental setup that was used in the experiments described in Chapter 5. For comparison, GNR FET and graphene sheet FET has been fabricated and measured. For GNR devices, 10 lines of approximately 20 nm width GNRs are used as an active channel (total channel width W = 200 nm) and channel length (L) is 520 nm. W of graphene sheet devices is 1 μm, and L = 1.98 μm. The devices are operated in air and under a flow of vapor, acetone. The devices are also evaluated again after the vapor flow is turned off.

Transfer characteristics of GNR FETs and graphene sheet FETs measured in air and acetone vapor are shown in Figure 6.2(a) and (b), respectively. The changes produced by polar vapors are reversible, similarly to the experiments mentioned in Chapter 5, as shown in Figure 6.3. In ambient air, GNR FETs have a huge hysteresis, a lower mobility and relatively larger Dirac voltage compared to graphene sheet FETs. Most likely these differences are due to the presence of additional defects – particularly edge defects and impurities.

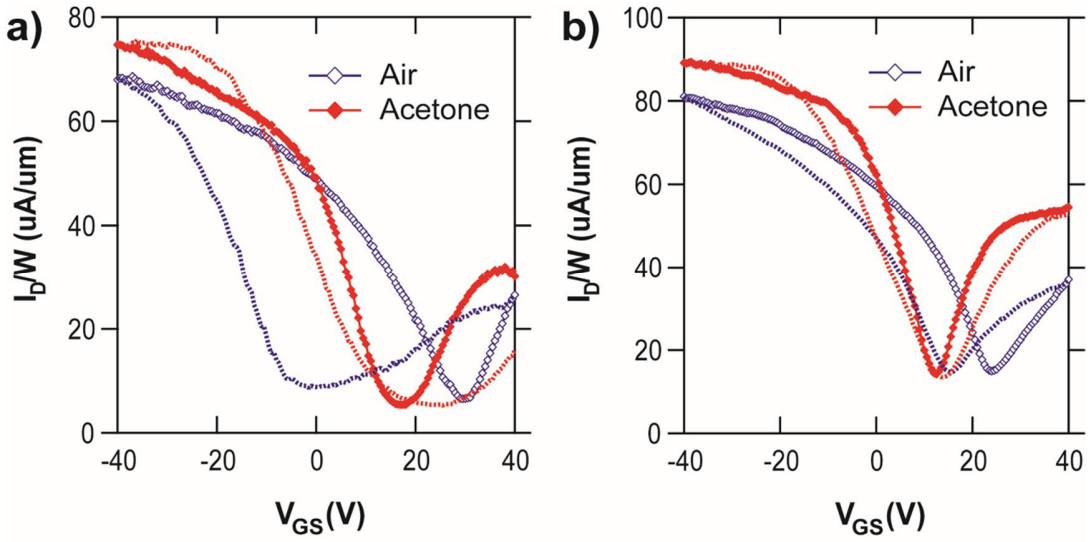

Figure 6.2: Transfer characteristics of GNR FET (a) with 10 GNRs of 20 nm width and graphene sheet FET (b) with W = 1 μm measured in ambient air and acetone vapor flow. L = 520 nm and 1.98 μm, respectively.

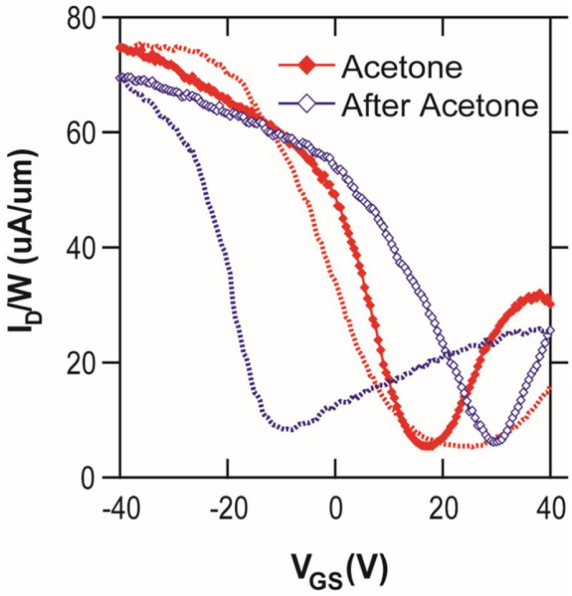

Figure 6.3: Transfer characteristics of GNR FET measured with acetone vapor flow and 1 min after the flow is turned off.

As represented in Figures 6.4(a) and (b), GNR FETs has a relatively smaller mobility compared to graphene sheet FETs, but the trend of improvement of mobility and reduction of residual carrier concentration under acetone flow is same. Figure 6.5(a) clearly demonstrates the advantages of polar molecules in the ambient. The on/off ratio if the GNR FETs is substantially improved as a result of exposure to acetone molecules. The hysteresis in GNR FETs exposed to acetone is greatly reduced, as shown in Figure 6.5(b). A hysteresis of FET is mainly related with trap states, which can hold charges for a while during sweeping gate voltage. Since most of traps are located at the edge of graphene area, the increased hysteresis could be a clear evidence of that GNR FETs are affected by edge defects much more than graphene sheet FETs. The Dirac voltage is also reduced in GNR FETs exposed to acetone. Graphene sheet devices also exhibit these trends qualitatively but not to the same degree as the GNR FETs [92]. This is because the polar molecules partially neutralize charged defects/impurities, similar to the effect discussed in Chapter 5.

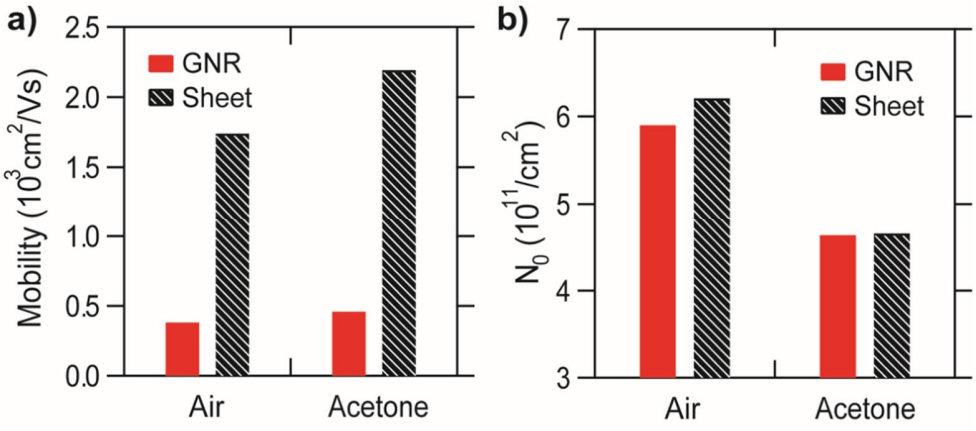

Figure 6.4: (a) Mobility and (b) carrier concentration of GNR and graphene sheet FETs measured in ambient air condition and with acetone vapor flow.

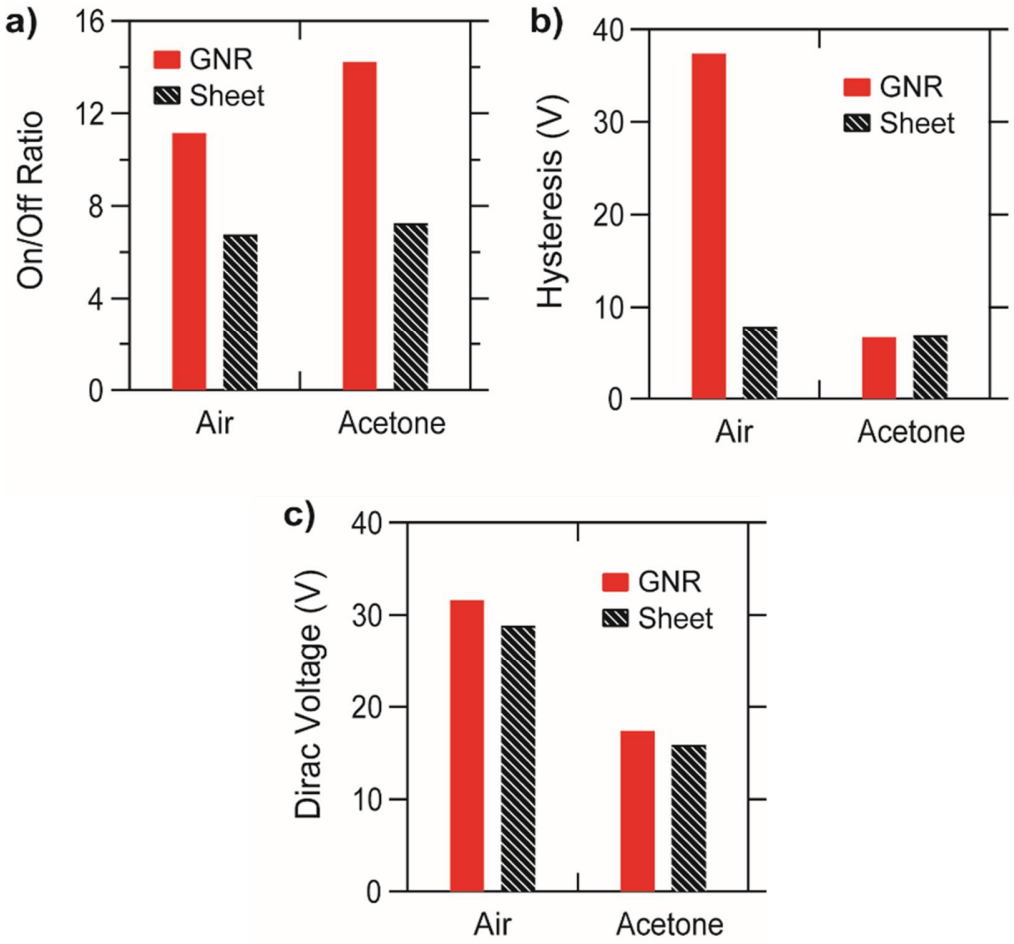

Figure 6.5: (a) On/Off Ratio, (b) Hysteresis and (c) Dirac voltage of GNR and graphene sheet FETs measured in ambient air condition and with acetone vapor flow. Hysteresis is calculated as a difference of gate voltage at maximum transconductance (g_m) depending on sweep direction.

6.4 CONCLUSION

In conclusion, the substantial improvement in electrical characteristics of GNR FETs under exposure to polar vapors has been investigated. For GNR FETs in general and for GNR patterned from large area CVD grown graphene in particular, defect engineering on edge states would be a key factor for the improvement of device properties. This work represents a promising approach as to how this can be accomplished.

Chapter 7. Conclusion

In this dissertation, a variety of studies on charge transport physics in polymer, graphene, and graphene nano-ribbon field-effect transistors has been demonstrated. First, a sub-threshold drift-limited regime conduction of high mobility polymer FETs has been investigated for the first time via accurate modeling process. In addition, based on modeling results, an accurate density of states of polymer FETs including deep trap states has been extracted. These result shows that density of trap states in sub-threshold regime should be calculated separately from above threshold regime. Diffusion-limited and drift-limited regime in sub-threshold region is separated by the level of interface trap density.

From accurate modeling results, a dominant charge transport mechanism in polymer FET under certain conditions has been also investigated. For high temperature and high carrier concentration operation, multiple trap and release (MTR) is the better fit to data. For low temperature and low carrier concentration operation, hopping transport models including various range hopping (VRH) and Gaussian disordered model (GDM) are adequate to explain modeled results.

A polaronic effect on charge transport in polymer FETs has been demonstrated. Polar molecules in atmosphere and dielectric, which behave as dipoles around a polymer semiconducting layer, has been investigated at the same time. Both dipoles from air and dielectric degrade the performance of polymer FETs, but the aspect of polaronic effects was slightly different for each case. If a polaronic effect from one side is weaker, then a polaronic effect from the other side becomes severe. In addition, dipoles in dielectric moves density of states curve uniformly, vice versa, dipoles in air mostly change density of states curve mostly in low energy area.

The effect of polar molecules on graphene field-effect transistors has been confirmed via polar vapor experiment, which is very effective and reversible system. By varying dipole moments of polar analytes, it was clear that highly polar molecules improve the electrical properties of graphene field-effect transistors. This result has showed the basic physics of the effect of fluoropolymer capping on graphene field-effect transistors.

Finally, the effect of polar molecules on graphene nano-ribbon field-effect transistors has been demonstrated. For graphene nano-ribbon devices, polar molecules showed a huge improvement in electrical characteristics compared to that of graphene sheet devices. Higher on/off ratio of graphene nano-ribbon was also attained. Especially, a huge hysteresis of graphene nano-ribbon transistors which is a clear evidence of edge defects, is greatly ameliorated via polar molecules, down to the similar level of that of graphene sheet transistors.

For future work, various circuit components could be realized with fluoropolymer capped graphene nano-ribbon transistors, thanks to high on/off ratio which is a suitable property for circuits. In addition, several different substrates and dielectrics including flexible materials could be applied for field-effect transistors. These devices with polymer and graphene nano-ribbon could be analyzed including sub-threshold conduction and charge transport mechanisms in transistors also could be investigated via a number of approaches that are demonstrated in this dissertation.

Appendix

List of Publications

1. **S. Kim** and A. Dodabalapur, "Polarization Effects from Ambient and Dielectric on Charge Transport in Polymer Field-effect Transistors," *Advanced Materials*, under review.

2. Y. Y. Illarionov, M. Waltl, G. Rzepa, J.-S. Kim, **S. Kim**, A. Dodabalapur, D. Akinwande and T. Grasser, "Long-Term Stability and Reliability of Black Phosphorus Field-Effect Transistors," *ACS nano* 10 (10), 9543-9549, 2016.

3. S. Jang, **S. Kim**, M. Geier, M. Hersam and A. Dodabalapur, "Inkjet Printed Carbon Nanotubes in Short Channel Field Effect Transistors: Influence of Nanotube Distortion and Gate Insulator Interface Modification," *Flexible and Printed Electronics* 1, 035001, 2016.

4. S. Rahimi, R. Ghosh, **S. Kim**, A. Dodabalapur, S. Banerjee and D. Akinwande, "The Positive Effects of Hydrophobic Fluoropolymers on the Electrical Properties of MoS2 Transistors," *Applied Science* 6, 236, 2016.

5. **S. Kim**, S. Park, D. Akinwande and A. Dodabalapur, "Electrical Performance Enhancement of 20 nm Scale Graphene Nanoribbon Field-Effect Transistors with Dipolar Molecules," *Device Research Conference (DRC) 74th Meeting*, Newark, DE, 2016.

6. **S. Kim**, B. C. Worley, P. J. Rossky, D. Akinwande and A. Dodabalapur, "Effect of Polar Vapor Molecules on the Electrical Characteristics of Monolayer Graphene Field-Effect transistors," *Electronic Materials Conference (EMC) 58th Meeting*, Newark, DE, 2016.

7. **S. Kim**, T.-J. Ha, P. Sonar and A. Dodabalapur, "Charge Transport above and below Threshold in High-Mobility polymer transistors," *Electronic Materials Conference (EMC) 58th Meeting*, Newark, DE, 2016.

8. **S. Kim**, T.-J. Ha, P. Sonar and A. Dodabalapur, "Charge Transport in Deep and Shallow States in a High-Mobility Polymer FET," *IEEE Transactions on Electron Devices* 63 (3), 1254-1259, 2016.

9. B. C. Worley*, **S. Kim***, S. Park, P. J. Rossky, D. Akinwande and A. Dodabalapur, "Dramatic Vapor-phase Modulation of the Characteristics of Graphene Field-Effect Transistors," *Physical Chemistry Chemical Physics* 17, 18426-18430, 2015. (*Equally contributed first authors)

10. **S. Kim**, T.-J. Ha, P. Sonar and A. Dodabalapur, "Sub-threshold Charge Transport in Polymer/Organic transistor," *The International Society of Optics and Photonics (SPIE) Optic + Photonics 2015 Meeting*, San Diego, CA, 2015. **(Invited)**

11. B. C. Worley, **S. Kim**, D. Akinwande, P. J. Rossky and A. Dodabalapur, "Mitigation of charged impurity effects in graphene field-effect transistors with polar organic molecules," *The International Society of Optics and Photonics (SPIE) Optic + Photonics 2015 Meeting*, San Diego, CA, 2015.

12. A. Dodabalapur, **S. Kim**, T.-J. Ha and P. Sonar, "Thin-Film Transistors based on Donor-Acceptor Polymers," *The Electrochemical Society (ECS) 227th Meeting*, Chicago, IL, 2015. **(Invited)**

13. **S. Kim**, T.-J. Ha, P. Sonar and A. Dodabalapur, "Density of Trap States in a Polymer Field-Effect Transistor," *The American Physical Society (APS) 2015 March Meeting*, San Antonio, TX, 2015.

14. B. C. Worley, **S. Kim**, S. Park, P. J. Rossky, D. Akinwande and A. Dodabalapur, "Graphene Transport under the Influence of Polar Molecules," *The American Physical Society (APS) 2015 March Meeting*, San Antonio, TX, 2015.

15. J.-S. Kim, Y. Liu, W. Zhu, **S. Kim**, D. Wu, L. Tao, A. Dodabalapur, K. Lai and D. Akinwande, "Toward Air-stable Multilayer Phosphorene Thin-films and Transistors," *Scientific Reports* 5, 8989, 2015.

16. **S. Kim**, T.-J. Ha, P. Sonar and A. Dodabalapur, "Density of Trap States in a Polymer Field-Effect Transistor," *Applied Physics Letters* 105 (13), 133302, 2014.

17. S. Noh, C. K. Suman, D. Lee, **S. Kim** and C. Lee, "Study of Buffer Layer Thickness on Bulk Heterojunction Solar Cell," *Journal of Nanoscience and Nanotechnology* 10 (10), 6815-6818, 2010.

18. C.-M. Kang, **S. Kim**, Y. Hong and C. Lee, "Frequency Analysis on Poly (3-hexylthiopene) Rectifier using Impedance Spectroscopy," *Thin Solid Films* 518 (2), 889-892, 2009.

19. **S. Kim**, H. Cho, Y. Hong and C. Lee, "Effect of Electrode Area on High Speed Characteristics over 1 MHz of Poly (3-hexylthiophene-2, 5-diyl) Diode with Inkjet-printed Ag Electrode," *Molecular Crystals and Liquid Crystals* 513 (1), 256-261, 2009.

20. H. Cho, **S. Kim**, Y. Hong and C. Lee, "Characteristics of Inverters using Pentacene Organic Thin Film Transistors with Printed Ag Electrodes," *Molecular Crystals and Liquid Crystals* 513 (1), 262-267, 2009.

21. C. K. Suman, J. Yun, **S. Kim**, S.-D. Lee and C. Lee, "AC Impedance Spectroscopic Studies of Transport Properties in Metal Oxide Doped α-NPD," *Current Applied Physics* 9 (5), 978-984, 2009.

22. C. K. Suman, S. Noh, **S. Kim**, S.-D. Lee, C. Lee, D. Lee and J. Park, "Electrical Impedance Studies of the Effect of a Buffer Layer on Organic Bulk-heterojunction Solar Cells," *Journal of the Korean Physical Society* 53 (6), 3278-3282, 2008.

23. S. Noh, **S. Kim**, J. Yang, C. Lee and J.-Y. Kim, "Investigation into the Thermal Annealing Effect on the Photovoltaic Properties of Organic Solar Cells based on CuPc/C60 Heterojunctions," *Journal of the Korean Physical Society* 53 (3), 1551-1555, 2008.

References

[1] A. Dodabalapur, "Organic and polymer transistors for electronics," *Materials Today,* vol. 9, pp. 24-30, 2006.

[2] Z. Bao, A. Dodabalapur, and A. J. Lovinger, "Soluble and processable regioregular poly(3-hexylthiophene) for thin film field-effect transistor applications with high mobility," *Applied Physics Letters,* vol. 69, pp. 4108-4110, 1996.

[3] B. Crone, A. Dodabalapur, Y. Y. Lin, R. W. Filas, Z. Bao, A. LaDuca*, et al.*, "Large-scale complementary integrated circuits based on organic transistors," *Nature,* vol. 403, pp. 521-523, 2000.

[4] H. Yan, Z. Chen, Y. Zheng, C. Newman, J. R. Quinn, F. Dotz*, et al.*, "A high-mobility electron-transporting polymer for printed transistors," *Nature,* vol. 457, pp. 679-686, 2009.

[5] I. McCulloch, M. Heeney, C. Bailey, K. Genevicius, I. MacDonald, M. Shkunov*, et al.*, "Liquid-crystalline semiconducting polymers with high charge-carrier mobility," *Nature Materials,* vol. 5, pp. 328-333, 2006.

[6] C. D. Sheraw, L. Zhou, J. R. Huang, D. J. Gundlach, T. N. Jackson, M. G. Kane*, et al.*, "Organic thin-film transistor-driven polymer-dispersed liquid crystal displays on flexible polymeric substrates," *Applied Physics Letters,* vol. 80, pp. 1088-1090, 2002.

[7] A. Dodabalapur, Z. Bao, A. Makhija, J. G. Laquindanum, V. R. Raju, Y. Feng*, et al.*, "Organic smart pixels," *Applied Physics Letters,* vol. 73, pp. 142-144, 1998.

[8] H. Sirringhaus, N. Tessler, and R. H. Friend, "Integrated Optoelectronic Devices Based on Conjugated Polymers," *Science,* vol. 280, pp. 1741-1744, 1998.

[9] B. Crone, A. Dodabalapur, A. Gelperin, L. Torsi, H. E. Katz, A. J. Lovinger*, et al.*, "Electronic sensing of vapors with organic transistors," *Applied Physics Letters,* vol. 78, pp. 2229-2231, 2001.

[10] B. K. Crone, A. Dodabalapur, R. Sarpeshkar, A. Gelperin, H. E. Katz, and Z. Bao, "Organic oscillator and adaptive amplifier circuits for chemical vapor sensing," *Journal of Applied Physics,* vol. 91, pp. 10140-10146, 2002.

[11] G. H. Gelinck, H. E. A. Huitema, E. van Veenendaal, E. Cantatore, L. Schrijnemakers, J. B. P. H. van der Putten*, et al.*, "Flexible active-matrix displays and shift registers based on solution-processed organic transistors," *Nature Materials,* vol. 3, pp. 106-110, 2004.

[12] Y. Watanabe and K. Kudo, "Flexible organic static induction transistors using pentacene thin films," *Applied Physics Letters,* vol. 87, p. 223505, 2005.

[13] B. Comiskey, J. D. Albert, H. Yoshizawa, and J. Jacobson, "An electrophoretic ink for all-printed reflective electronic displays," *Nature,* vol. 394, pp. 253-255, 1998.

[14] C. D. Dimitrakopoulos and P. R. L. Malenfant, "Organic Thin Film Transistors for Large Area Electronics," *Advanced Materials,* vol. 14, pp. 99-117, 2002.

[15] T.-J. Ha, P. Sonar, and A. Dodabalapur, "Charge transport study of high mobility polymer thin-film transistors based on thiophene substituted diketopyrrolopyrrole copolymers," *Physical Chemistry Chemical Physics,* vol. 15, pp. 9735-9741, 2013.

[16] T.-J. Ha, P. Sonar, and A. Dodabalapur, "Improved Performance in Diketopyrrolopyrrole-Based Transistors with Bilayer Gate Dielectrics," *ACS Applied Materials & Interfaces,* vol. 6, pp. 3170-3175, 2014.

[17] H.-R. Tseng, L. Ying, B. B. Y. Hsu, L. A. Perez, C. J. Takacs, G. C. Bazan*, et al.*, "High Mobility Field Effect Transistors Based on Macroscopically Oriented Regioregular Copolymers," *Nano Letters,* vol. 12, pp. 6353-6357, 2012.

[18] P. Sonar, S. P. Singh, Y. Li, M. S. Soh, and A. Dodabalapur, "A Low-Bandgap Diketopyrrolopyrrole-Benzothiadiazole-Based Copolymer for High-Mobility Ambipolar Organic Thin-Film Transistors," *Advanced Materials,* vol. 22, pp. 5409-5413, 2010.

[19] I. Kang, H.-J. Yun, D. S. Chung, S.-K. Kwon, and Y.-H. Kim, "Record High Hole Mobility in Polymer Semiconductors via Side-Chain Engineering," *Journal of the American Chemical Society,* vol. 135, pp. 14896-14899, 2013.

[20] J. Lee, A. R. Han, H. Yu, T. J. Shin, C. Yang, and J. H. Oh, "Boosting the Ambipolar Performance of Solution-Processable Polymer Semiconductors via Hybrid Side-Chain Engineering," *Journal of the American Chemical Society,* vol. 135, pp. 9540-9547, 2013.

[21] H. Chen, Y. Guo, G. Yu, Y. Zhao, J. Zhang, D. Gao*, et al.*, "Highly π-Extended Copolymers with Diketopyrrolopyrrole Moieties for High-Performance Field-Effect Transistors," *Advanced Materials,* vol. 24, pp. 4618-4622, 2012.

[22] J. H. Kim, D. H. Lee, D. S. Yang, D. U. Heo, K. H. Kim, J. Shin*, et al.*, "Novel Polymer Nanowire Crystals of Diketopyrrolopyrrole-Based Copolymer with Excellent Charge Transport Properties," *Advanced Materials,* vol. 25, pp. 4102-4106, 2013.

[23] D. Akinwande, N. Petrone, and J. Hone, "Two-dimensional flexible nanoelectronics," *Nature Communications,* vol. 5, 2014.

[24] Q. H. Wang, K. Kalantar-Zadeh, A. Kis, J. N. Coleman, and M. S. Strano, "Electronics and optoelectronics of two-dimensional transition metal dichalcogenides," *Nature Nanotechnology,* vol. 7, pp. 699-712, 2012.

[25] S. Z. Butler, S. M. Hollen, L. Cao, Y. Cui, J. A. Gupta, H. R. Gutiérrez*, et al.*, "Progress, Challenges, and Opportunities in Two-Dimensional Materials Beyond Graphene," *ACS Nano,* vol. 7, pp. 2898-2926, 2013.

[26] I. Meric, C. R. Dean, N. Petrone, W. Lei, J. Hone, P. Kim*, et al.*, "Graphene Field-Effect Transistors Based on Boron Nitride Dielectrics," *Proceedings of the IEEE,* vol. 101, pp. 1609-1619, 2013.

[27] H. Fang, S. Chuang, T. C. Chang, K. Takei, T. Takahashi, and A. Javey, "High-Performance Single Layered WSe2 p-FETs with Chemically Doped Contacts," *Nano Letters,* vol. 12, pp. 3788-3792, 2012.

[28] G.-H. Lee, Y.-J. Yu, X. Cui, N. Petrone, C.-H. Lee, M. S. Choi*, et al.*, "Flexible and Transparent MoS2 Field-Effect Transistors on Hexagonal Boron Nitride-Graphene Heterostructures," *ACS Nano,* vol. 7, pp. 7931-7936, 2013.

[29] H.-Y. Chang, S. Yang, J. Lee, L. Tao, W.-S. Hwang, D. Jena*, et al.*, "High-Performance, Highly Bendable MoS2 Transistors with High-K Dielectrics for Flexible Low-Power Systems," *ACS Nano,* vol. 7, pp. 5446-5452, 2013.

[30] J. Lee, T.-J. Ha, H. Li, K. N. Parrish, M. Holt, A. Dodabalapur*, et al.*, "25 GHz Embedded-Gate Graphene Transistors with High-K Dielectrics on Extremely Flexible Plastic Sheets," *ACS Nano,* vol. 7, pp. 7744-7750, 2013.

[31] S. Das, R. Gulotty, A. V. Sumant, and A. Roelofs, "All Two-Dimensional, Flexible, Transparent, and Thinnest Thin Film Transistor," *Nano Letters,* vol. 14, pp. 2861-2866, 2014.

[32] S. Park, S. H. Shin, M. N. Yogeesh, A. L. Lee, S. Rahimi, and D. Akinwande, "Extremely High-Frequency Flexible Graphene Thin-Film Transistors," *IEEE Electron Device Letters,* vol. 37, pp. 512-515, 2016.

[33] W. Zhu, S. Park, M. N. Yogeesh, K. M. McNicholas, S. R. Bank, and D. Akinwande, "Black Phosphorus Flexible Thin Film Transistors at Gighertz Frequencies," *Nano Letters,* vol. 16, pp. 2301-2306, 2016.

[34] J. A. Rogers, Z. Bao, K. Baldwin, A. Dodabalapur, B. Crone, V. R. Raju*, et al.*, "Paper-like electronic displays: Large-area rubber-stamped plastic sheets of electronics and microencapsulated electrophoretic inks," *Proceedings of the National Academy of Sciences,* vol. 98, pp. 4835-4840, 2001.

[35] G. Horowitz, "Organic Field-Effect Transistors," *Advanced Materials,* vol. 10, pp. 365-377, 1998.

[36] V. Coropceanu, J. Cornil, D. A. da Silva Filho, Y. Olivier, R. Silbey, and J.-L. Brédas, "Charge Transport in Organic Semiconductors," *Chemical Reviews,* vol. 107, pp. 926-952, 2007.

[37] R. J. Chesterfield, C. R. Newman, T. M. Pappenfus, P. C. Ewbank, M. H. Haukaas, K. R. Mann*, et al.*, "High Electron Mobility and Ambipolar Transport in Organic Thin-Film Transistors Based on a π-Stacking Quinoidal Terthiophene," *Advanced Materials,* vol. 15, pp. 1278-1282, 2003.

[38] N. F. Mott, "Conduction in glasses containing transition metal ions," *Journal of Non-Crystalline Solids,* vol. 1, pp. 1-17, 1968.

[39] N. Tessler, Y. Preezant, N. Rappaport, and Y. Roichman, "Charge Transport in Disordered Organic Materials and Its Relevance to Thin-Film Devices: A Tutorial Review," *Advanced Materials,* vol. 21, pp. 2741-2761, 2009.

[40] P. Stallinga, "Electronic Transport in Organic Materials: Comparison of Band Theory with Percolation/(Variable Range) Hopping Theory," *Advanced Materials,* vol. 23, pp. 3356-3362, 2011.

[41] G. Paasch, T. Lindner, and S. Scheinert, "Variable range hopping as possible origin of a universal relation between conductivity and mobility in disordered organic semiconductors," *Synthetic Metals,* vol. 132, pp. 97-104, 2002.

[42] H. Bässler, "Localized states and electronic transport in single component organic solids with diagonal disorder," *Physica Status Solidi (b),* vol. 107, pp. 9-54, 1981.

[43] P. E. Parris, V. M. Kenkre, and D. H. Dunlap, "Nature of Charge Carriers in Disordered Molecular Solids: Are Polarons Compatible with Observations?," *Physical Review Letters,* vol. 87, p. 126601, 2001.

[44] I. I. Fishchuk, V. I. Arkhipov, A. Kadashchuk, P. Heremans, and H. Bässler, "Analytic model of hopping mobility at large charge carrier concentrations in disordered organic semiconductors: Polarons versus bare charge carriers," *Physical Review B,* vol. 76, p. 045210, 2007.

[45] W. F. Pasveer, J. Cottaar, C. Tanase, R. Coehoorn, P. A. Bobbert, P. W. M. Blom*, et al.*, "Unified Description of Charge-Carrier Mobilities in Disordered Semiconducting Polymers," *Physical Review Letters,* vol. 94, p. 206601, 2005.

[46] H. Sirringhaus, "Device Physics of Solution-Processed Organic Field-Effect Transistors," *Advanced Materials,* vol. 17, pp. 2411-2425, 2005.

[47] R. Noriega, J. Rivnay, K. Vandewal, F. P. V. Koch, N. Stingelin, P. Smith, *et al.*, "A general relationship between disorder, aggregation and charge transport in conjugated polymers," *Nature Materials,* vol. 12, pp. 1038-1044, 2013.

[48] D. Venkateshvaran, M. Nikolka, A. Sadhanala, V. Lemaur, M. Zelazny, M. Kepa, *et al.*, "Approaching disorder-free transport in high-mobility conjugated polymers," *Nature,* vol. 515, pp. 384-388, 2014.

[49] S. Lee, S. Jeon, and A. Nathan, "Modeling Sub-Threshold Current?Voltage Characteristicsin Thin Film Transistors," *Journal of Display Technology,* vol. 9, pp. 883-889, 2013.

[50] S. Kim, T. J. Ha, P. Sonar, and A. Dodabalapur, "Charge Transport in Deep and Shallow States in a High-Mobility Polymer FET," *IEEE Transactions on Electron Devices,* vol. 63, pp. 1254-1259, 2016.

[51] I. G. Hill, A. Kahn, Z. G. Soos, and J. R. A. Pascal, "Charge-separation energy in films of π-conjugated organic molecules," *Chemical Physics Letters,* vol. 327, pp. 181-188, 2000.

[52] D. Duarte, D. Sharma, B. Cobb, and A. Dodabalapur, "Charge transport and trapping in organic field effect transistors exposed to polar analytes," *Applied Physics Letters,* vol. 98, p. 133302, 2011.

[53] I. N. Hulea, S. Fratini, H. Xie, C. L. Mulder, N. N. Iossad, G. Rastelli, *et al.*, "Tunable Frohlich polarons in organic single-crystal transistors," *Nature Materials,* vol. 5, pp. 982-986, 2006.

[54] L. Torsi, A. J. Lovinger, B. Crone, T. Someya, A. Dodabalapur, H. E. Katz, *et al.*, "Correlation between Oligothiophene Thin Film Transistor Morphology and Vapor Responses," *The Journal of Physical Chemistry B,* vol. 106, pp. 12563-12568, 2002.

[55] S. Adam, E. H. Hwang, V. M. Galitski, and S. Das Sarma, "A self-consistent theory for graphene transport," *Proceedings of the National Academy of Sciences of the United States of America,* vol. 104, pp. 18392-18397, 2007.

[56] S. Das Sarma, S. Adam, E. H. Hwang, and E. Rossi, "Electronic transport in two-dimensional graphene," *Reviews of Modern Physics,* vol. 83, pp. 407-470, 2011.

[57] K. S. Novoselov, A. K. Geim, S. V. Morozov, D. Jiang, M. I. Katsnelson, I. V. Grigorieva, *et al.*, "Two-dimensional gas of massless Dirac fermions in graphene," *Nature,* vol. 438, pp. 197-200, 2005.

[58] J.-H. Chen, C. Jang, S. Xiao, M. Ishigami, and M. S. Fuhrer, "Intrinsic and extrinsic performance limits of graphene devices on SiO2," *Nature Nanotechnology,* vol. 3, pp. 206-209, 2008.

[59] P. Avouris, "Graphene: Electronic and Photonic Properties and Devices," *Nano Letters,* vol. 10, pp. 4285-4294, 2010.

[60] C. Jang, S. Adam, J. H. Chen, E. D. Williams, S. Das Sarma, and M. S. Fuhrer, "Tuning the Effective Fine Structure Constant in Graphene: Opposing Effects of Dielectric Screening on Short- and Long-Range Potential Scattering," *Physical Review Letters,* vol. 101, p. 146805, 2008.

[61] E. H. Hwang, S. Adam, and S. D. Sarma, "Carrier Transport in Two-Dimensional Graphene Layers," *Physical Review Letters,* vol. 98, p. 186806, 2007.

[62] T.-J. Ha, J. Lee, S. F. Chowdhury, D. Akinwande, P. J. Rossky, and A. Dodabalapur, "Transformation of the Electrical Characteristics of Graphene Field-Effect Transistors with Fluoropolymer," *ACS Applied Materials & Interfaces,* vol. 5, pp. 16-20, 2013.

[63] T. J. Ha, J. Lee, D. Akinwande, and A. Dodabalapur, "The Restorative Effect of Fluoropolymer Coating on Electrical Characteristics of Graphene Field-Effect Transistors," *Electron Device Letters, IEEE,* vol. 34, pp. 559-561, 2013.

[64] J. H. Chen, C. Jang, S. Adam, M. S. Fuhrer, E. D. Williams, and M. Ishigami, "Charged-impurity scattering in graphene," *Nature Physics,* vol. 4, pp. 377-381, 2008.

[65] W. H. Lee, J. W. Suk, J. Lee, Y. Hao, J. Park, J. W. Yang*, et al.*, "Simultaneous Transfer and Doping of CVD-Grown Graphene by Fluoropolymer for Transparent Conductive Films on Plastic," *ACS Nano,* vol. 6, pp. 1284-1290, 2012.

[66] M. Y. Han, B. Özyilmaz, Y. Zhang, and P. Kim, "Energy Band-Gap Engineering of Graphene Nanoribbons," *Physical Review Letters,* vol. 98, p. 206805, 2007.

[67] K. Wakabayashi, M. Fujita, H. Ajiki, and M. Sigrist, "Electronic and magnetic properties of nanographite ribbons," *Physical Review B,* vol. 59, pp. 8271-8282, 1999.

[68] K. Nakada, M. Fujita, G. Dresselhaus, and M. S. Dresselhaus, "Edge state in graphene ribbons: Nanometer size effect and edge shape dependence," *Physical Review B,* vol. 54, pp. 17954-17961, 1996.

[69] T. C. Li and S.-P. Lu, "Quantum conductance of graphene nanoribbons with edge defects," *Physical Review B,* vol. 77, p. 085408, 2008.

[70] M. P. Anantram and T. R. Govindan, "Conductance of carbon nanotubes with disorder: A numerical study," *Physical Review B,* vol. 58, pp. 4882-4887, 1998.

[71] S. Banerjee, M. Sardar, N. Gayathri, A. K. Tyagi, and B. Raj, "Conductivity landscape of highly oriented pyrolytic graphite surfaces containing ribbons and edges," *Physical Review B,* vol. 72, p. 075418, 2005.

[72] S. Kim, T.-J. Ha, P. Sonar, and A. Dodabalapur, "Density of trap states in a polymer field-effect transistor," *Applied Physics Letters,* vol. 105, p. 133302, 2014.

[73] L. Torsi, A. Dodabalapur, L. J. Rothberg, A. W. P. Fung, and H. E. Katz, "Charge transport in oligothiophene field-effect transistors," *Physical Review B,* vol. 57, pp. 2271-2275, 1998.

[74] V. Podzorov, E. Menard, A. Borissov, V. Kiryukhin, J. A. Rogers, and M. E. Gershenson, "Intrinsic Charge Transport on the Surface of Organic Semiconductors," *Physical Review Letters,* vol. 93, p. 086602, 2004.

[75] A. Salleo, "Charge transport in polymeric transistors," *Materials Today,* vol. 10, pp. 38-45, 2007.

[76] L. Dunn, B. Cobb, D. Reddy, and A. Dodabalapur, "Dynamic characterization of charge transport in organic and polymer transistors," *Applied Physics A,* vol. 95, pp. 153-158, 2009.

[77] D. V. Lang, X. Chi, T. Siegrist, A. M. Sergent, and A. P. Ramirez, "Amorphouslike Density of Gap States in Single-Crystal Pentacene," *Physical Review Letters,* vol. 93, p. 086802, 2004.

[78] W.-y. So, D. V. Lang, V. Y. Butko, X. Chi, J. C. Lashley, and A. P. Ramirez, "Dependence of mobility on density of gap states in organics by GAMEaS-gate modulated activation energy spectroscopy," *Journal of Applied Physics,* vol. 104, 2008.

[79] W. L. Kalb, K. Mattenberger, and B. Batlogg, "Oxygen-related traps in pentacene thin films: Energetic position and implications for transistor performance," *Physical Review B,* vol. 78, p. 035334, 2008.

[80] W. L. Kalb and B. Batlogg, "Calculating the trap density of states in organic field-effect transistors from experiment: A comparison of different methods," *Physical Review B,* vol. 81, p. 035327, 2010.

[81] T. J. Ha, P. Sonar, and A. Dodabalapur, "Solution-Processed Dual-Gate Polymer Field-Effect Transistors for Display Applications," *Display Technology, Journal of,* vol. 9, pp. 710-714, 2013.

[82] T.-J. Ha, P. Sonar, B. Cobb, and A. Dodabalapur, "Charge transport and density of trap states in balanced high mobility ambipolar organic thin-film transistors," *Organic Electronics,* vol. 13, pp. 136-141, 2012.

[83] M. McDowell, I. G. Hill, J. E. McDermott, S. L. Bernasek, and J. Schwartz, "Improved organic thin-film transistor performance using novel self-assembled monolayers," *Applied Physics Letters,* vol. 88, 2006.

[84] M. Shur, M. Hack, and J. G. Shaw, "A new analytic model for amorphous silicon thin-film transistors," *Journal of Applied Physics,* vol. 66, pp. 3371-3380, 1989.

[85] G. Horowitz, M. E. Hajlaoui, and R. Hajlaoui, "Temperature and gate voltage dependence of hole mobility in polycrystalline oligothiophene thin film transistors," *Journal of Applied Physics,* vol. 87, pp. 4456-4463, 2000.

[86] M. C. J. M. Vissenberg and M. Matters, "Theory of the field-effect mobility in amorphous organic transistors," *Physical Review B,* vol. 57, pp. 12964-12967, 1998.

[87] A. Miller and E. Abrahams, "Impurity Conduction at Low Concentrations," *Physical Review,* vol. 120, pp. 745-755, 1960.

[88] C.-G. Lee, B. Cobb, and A. Dodabalapur, "Band transport and mobility edge in amorphous solution-processed zinc tin oxide thin-film transistors," *Applied Physics Letters,* vol. 97, p. 203505, 2010.

[89] H.-R. Tseng, H. Phan, C. Luo, M. Wang, L. A. Perez, S. N. Patel*, et al.*, "High-Mobility Field-Effect Transistors Fabricated with Macroscopic Aligned Semiconducting Polymers," *Advanced Materials,* vol. 26, pp. 2993-2998, 2014.

[90] S. Kim and A. Dodabalapur, "Polarization Effects from Ambient and Dielectric on Charge Transport in Polymer Field-effect Transistors," *Advanced Materials,* under review.

[91] C.-G. Lee and A. Dodabalapur, "Solution-Processed High-k Dielectric, ZrO2, and Integration in Thin-Film Transistors," *Journal of Electronic Materials,* vol. 41, pp. 895-898, 2012.

[92] B. C. Worley, S. Kim, S. Park, P. J. Rossky, D. Akinwande, and A. Dodabalapur, "Dramatic vapor-phase modulation of the characteristics of graphene field-effect transistors," *Physical Chemistry Chemical Physics,* vol. 17, pp. 18426-18430, 2015.

[93] B. Fallahazad, S. Kim, L. Colombo, and E. Tutuc, "Dielectric thickness dependence of carrier mobility in graphene with HfO2 top dielectric," *Applied Physics Letters,* vol. 97, p. 123105, 2010.

[94] A. K. M. Newaz, Y. S. Puzyrev, B. Wang, S. T. Pantelides, and K. I. Bolotin, "Probing charge scattering mechanisms in suspended graphene by varying its dielectric environment," *Nature Communications,* vol. 3, p. 734, 2012.

[95] L. Tao, J. Lee, H. Chou, M. Holt, R. S. Ruoff, and D. Akinwande, "Synthesis of High Quality Monolayer Graphene at Reduced Temperature on Hydrogen-Enriched Evaporated Copper (111) Films," *ACS Nano,* vol. 6, pp. 2319-2325, 2012.

[96] J. Lee, L. Tao, Y. Hao, R. S. Ruoff, and D. Akinwande, "Embedded-gate graphene transistors for high-mobility detachable flexible nanoelectronics," *Applied Physics Letters,* vol. 100, p. 152104, 2012.

[97] R. D. Nelson Jr, D. R. Lide Jr, and A. A. Maryott, "Selected values of electric dipole moments for molecules in the gas phase," DTIC Document 1967.

[98] S. Kim, J. Nah, I. Jo, D. Shahrjerdi, L. Colombo, Z. Yao*, et al.*, "Realization of a high mobility dual-gated graphene field-effect transistor with Al2O3 dielectric," *Applied Physics Letters,* vol. 94, p. 062107, 2009.

[99] J. H. Chen, C. Jang, M. Ishigami, S. Xiao, W. G. Cullen, E. D. Williams*, et al.*, "Diffusive charge transport in graphene on SiO2," *Solid State Communications,* vol. 149, pp. 1080-1086, 2009.

[100] S. Kim, S. Park, D. Akinwande, and A. Dodabalapur, "Electrical performance enhancement of 20 nm scale graphene nanoribbon field-effect transistors with dipolar molecules," in *Device Research Conference (DRC), 2016 74th Annual*, 2016, pp. 1-2.

[101] X. Li, X. Wang, L. Zhang, S. Lee, and H. Dai, "Chemically Derived, Ultrasmooth Graphene Nanoribbon Semiconductors," *Science,* vol. 319, pp. 1229-1232, 2008.

Vita

Seohee Kim was born in Incheon, Korea. He graduated from Yeonsu High School in Incheon in 2003, with the honor of top of the city in Korean SAT. He attended Seoul National University in Seoul, Korea with National Science and Engineering Undergraduate Scholarship for undergraduate course and Samsung Scholarship for graduate course. He earned a Bachelor of Science in Electrical Engineering and a Master of Science in Electrical Engineering and Computer Science in 2007 and 2009, respectively. He was a memory circuit design engineer at Samsung Electronics from February 2009 to May 2012. He began his doctoral research in Electrical and Computer Engineering at The University of Texas at Austin in 2012. His doctoral research on the charge transport physics in polymer and graphene field-effect transistors has been supervised by Professor Ananth Dodabalapur.

Permanent email: seohk03@gmail.com

This dissertation was typed by Seohee Kim.